Indoor Burning of Arabian Incense Generates Abundant Ultrafine Particles with Strong Oxidative Potential

Liyuan Zhou[1,2*], Zhancong Liang[2], Wei Xu[1], Ru-Jin Huang[3], Patrick K. H. Lee[4] and Chak K. Chan[2*]

[1]State Key Laboratory of Advanced Environmental Technology, Institute of Urban Environment, Chinese Academy of Sciences, Xiamen 361021, China
[2]Division of Biological and Environmental Science and Engineering, King Abdullah University of Science and Technology, Thuwal, Jeddah 23955-6900, Kingdom of Saudi Arabia
[3]State Key Laboratory of Loess Science, Institute of Earth Environment, Chinese Academy of Sciences, Xi'an 710061, China
[4]School of Energy and Environment, City University of Hong Kong, Hong Kong SAR, China

Correspondence to: Liyuan Zhou (lyzhou@iue.ac.cn) and Chak K. Chan (chak.chan@kaust.edu.sa)

Abstract. Arabian incense (Bakhoor) burning is a widely practiced fragrancing and ceremonial activity, yet how the Bakhoor composition controls particle emissions and oxidative potential remains poorly constrained, especially under repeated use in low-ventilation settings. Here we characterized emissions from Bakhoor burning in a controlled chamber using a charcoal-assisted heating configuration representative of common practice and quantified aerosol oxidative potential using complementary acellular dithiothreitol (DTT) activity and a macrophage-based intracellular oxidative-stress response, with smoldering sidestream cigarette smoke as a protocol-matched indoor combustion reference. Normalized by the initial Bakhoor mass per burn, Bakhoor burning produced particle mass and number emission rates of 670-1690 μg min^{-1} g^{-1} and (6-7) × 10^{11} particles min^{-1} g^{-1}, respectively. Ultrafine particles contributed 70-75% of the total particle number, and their emission rates substantially exceeded those from sidestream cigarette smoke. Across Bakhoor materials, emission magnitude followed a nonlinear power-law relationship with the loading of the hexane-soluble fraction, indicating that this fraction is an important control on particle production. In the acellular assay, the water-soluble particle mass-normalized DTT consumption rate ($OP_{DTT,m}^{WS}$) was approximately 32 pmol min^{-1} μg^{-1}, modestly lower than that of cigarette smoke particles, whereas Bakhoor burning particles elicited stronger intracellular oxidative-stress responses. Ozone aging increased oxidative potential for both sources, and the acellular and cellular responses remained evident after aging equivalent to days of indoor exposure. Overall, Bakhoor burning represents a previously underrecognized source of ultrafine aerosol with substantial oxidative potential.

1. Introduction

Global exposure assessments indicate that people spend approximately 60-90% of their time indoors (Sadoun et al., 2016; Pillarisetti et al., 2022), making indoor environments an important setting for air pollutant exposure. In arid regions such as the Middle East, this percentage can approach 100% (Sadoun et al., 2016), driven by extended periods of extreme heat and limited outdoor comfort. Despite this high exposure potential, indoor air quality has historically received less scientific and regulatory attention than outdoor pollution (Cincinelli and Martellini, 2017). Indoor air is shaped by both outdoor infiltration and indoor activities, with combustion-related processes often contributing substantially to particle exposure (Gligorovski and Abbatt, 2018). While major indoor combustion sources such as tobacco smoke and household solid-fuel use have been widely studied (Wang et al., 2018a), other routine combustion-based fragrancing and ceremonial practices remain comparatively under-characterized as particle sources.

A prominent example is the burning of Arabian incense (Bakhoor), a widely practiced fragrancing and ceremonial activity in the Middle East and other regions, in which a mixture of perfumed wood chips soaked with additives is heated on charcoal. In addition to the aromatic wood chips, Bakhoor materials often contain scented oils, resins, and botanical additives such as herbs and flowers (Wahab and Mostafa, 2007), forming a chemically complex mixture that can generate condensable precursors upon thermal degradation. Because Bakhoor is typically heated on smoldering charcoal, both the Bakhoor material and the ignition source can contribute to particle formation. Bakhoor burning commonly occurs indoors, often in enclosed spaces with limited ventilation, and is embedded in daily routines as well as religious and social gatherings. In Jazan, Saudi Arabia, 98% of households report regularly burning Bakhoor indoors (Jareebi et al., 2024). Frequent incense use has also been reported in Gulf regions (Yeatts et al., 2012), while household incense burning is likewise prevalent in parts of Asia (Pan et al., 2014; Zhao et al., 2025). This widespread use indicates that combustion-based fragrancing and ceremonial practices are not only regionally important, but also relevant to a broader class of indoor combustion sources. For such sources, quantitative descriptors such as source strength, particle size distribution, and particle reactivity are important for understanding emission characteristics and how they vary with source composition and burning conditions (Kuye and Kumar, 2023). Ultrafine particles are often of particular interest because of their importance to particle number emissions and their potential sensitivity to source and combustion conditions (Shen et al., 2017).

Previous studies have provided evidence that Bakhoor and related incense smoke can have adverse respiratory and toxicological effects. Epidemiological work has linked domestic bakhoor use with respiratory symptoms. For example, Al-Rawas et al. (2009) reported that Arabian incense burning was a common trigger of wheezing among asthmatic children in Oman. Cohen et al. (2013) characterized particles and gases emitted from United Arab Emirates (UAE) incense burning under indoor chamber conditions and reported inflammatory responses in exposed human lung cells, providing an important prior hazard-assessment study of Arabian incense smoke. The chemical complexity of Bakhoor further complicates source interpretation. Elsayed et al. (2016) reported that raw, unburned Bakhoor materials contain a chemically complex mixture of organic constituents, including nitrogen-containing and other additive-related species. However, the composition of particles emitted during Bakhoor burning can differ substantially from the raw-material profile because thermochemical processing

during heating and pyrolysis can transform the formulation and generate new condensable products that partition to the particle phase. Dalibalta et al. (2015) provided preliminary indications of potential concern in Bakhoor smoke by noting the presence of compounds classified as carcinogenic, toxic, and/or respiratory irritants; however, the evidence was not linked to size-resolved emissions or dose-relevant particle metrics. Alarifi et al. (2004) further reported structural changes in pneumocytes following repeated animal exposure to Bakhoor smoke. Together, these studies establish a health-relevant basis for concern. However, the particle-level basis for assessing exposure from practical Bakhoor burning remains insufficiently constrained, including how emissions vary with source configuration and product composition, and how the emitted particles express oxidative potential before and after indoor-relevant aging. These gaps motivate a quantitative particle-based evaluation of Bakhoor burning.

Here, we characterize particle emissions and oxidative responses of Bakhoor burning in a controlled chamber, using smoldering sidestream cigarette smoke as a protocol-matched indoor combustion reference (Chen and Zhao, 2024). Real-time particle number and mass concentrations and size distributions were measured using a scanning mobility particle sizer, and size-resolved emission factors were quantified. Particular attention was given to ultrafine particles (UFPs, <100 nm) because of their high respiratory deposition efficiency and potential relevance to systemic health effects (Oberdörster et al., 2005). Control experiments were performed to quantify the respective contributions of the Bakhoor material and the ignition charcoal to emitted particle size distributions and emission factors. Oxidative responses were evaluated using two complementary approaches commonly applied in atmospheric and exposure research (Seo et al., 2025). These included acellular oxidative potential quantified by the dithiothreitol (DTT) assay and cellular responses assessed via intracellular oxidative-stress response and cell viability in alveolar macrophages. To probe potential chemical drivers, particle extracts were analyzed offline using high-performance liquid chromatography coupled with high-resolution mass spectrometry, and compositional metrics were examined in relation to DTT activity. Changes in chemical composition and associated oxidative responses of Bakhoor burning particles were also evaluated following ozone exposure as an additional probe of post-emission processing. This work aims to better constrain the size-resolved emissions, source contributions, and oxidative responses of particles emitted from Bakhoor burning.

2. Methods

2.1 Generation and collection of particles from Bakhoor burning and sidestream cigarette smoke

All burning experiments were conducted inside a custom-built acrylic chamber (50 × 50 × 50 cm). Three commercially available Bakhoor products were purchased from local markets in Saudi Arabia, selected based on consumer popularity. For each experiment, 1 g of Bakhoor was placed onto a smoldering charcoal briquette, consistent with common household practice. The charcoal was a commercially available quick-lighting type typically used for Bakhoor burning. Charcoal-only burns were conducted under the same chamber configuration to quantify emissions attributable to the ignition source. As a protocol-matched indoor combustion reference, smoldering sidestream cigarette smoke was generated in the same chamber to provide a stable and continuous particle stream. Although this approach differs from puffing-based protocols, it improves

reproducibility and has been used in prior emission studies (Ott et al., 2021; Wu et al., 2012). Once Bakhoor was placed on the smoldering charcoal, visible smoke generation began immediately and typically persisted for approximately 20 min. The chamber was operated under a steady-state flow-through mode with purified air supplied at 20 L min^{-1}. Size-resolved particle number concentrations were continuously measured using a Scanning Electrical Mobility Spectrometer (SEMS; Model 2100, Brechtel Manufacturing Inc.) over a mobility diameter range of 10–500 nm. Larger particles (500–2500 nm) were quantified using an optical particle counter (OPC; Brechtel Manufacturing Inc.). Prior to each experiment, background particle concentrations in the chamber were reduced to <1 particle cm^{-3}. Particle number size distributions from the SEMS and OPC were converted to mass concentrations assuming an effective particle density of 1 g cm^{-3}. This value has been used in previous indoor particle and combustion-emission studies to estimate particle mass from size distributions (Wallace, 2006; Klosterköther et al., 2021) and is close to the reported density of incense smoke particles, approximately 1.1 g cm^{-3} (Ji et al., 2010). Fresh combustion aerosols may have source- and size-dependent effective densities because of differences in morphology and composition. In addition to real-time measurements, aerosol samples were collected on 47 mm quartz and PTFE filters, each at approximately 6 L min^{-1} for offline chemical analysis. Quartz filters were pre-baked at 550 °C for 12 h to minimize background organic contamination.

2.2 Emission rate calculations

Particle mass emission rates (E, μg min^{-1}) were quantified using a size-resolved material-balance approach (Wang and Chan, 2023; Jiang et al., 2021), where particle losses were treated separately for each size bin. The chamber was continuously mixed using two internal fans, and emission rates were therefore derived using a well-mixed flow-through chamber mass-balance framework. For analysis, particles were grouped into the following diameter bins: 10-100, 100-200, 200-300, 300-400, 400-500, 500-1000, 1000-1500, 1500-2000, and 2000-2500 nm.

For each size bin *i*, the time-dependent mass balance in the well-mixed chamber is

$$V\frac{dC_i}{dt} = -F \times C_i + E_i - k_i \times V \times C_i, \quad \text{(Eq. 1)}$$

where V is the volume of the chamber (m^3), C_i is the mass concentration of particles in size bin i (μg m^{-3}), F is the outlet airflow rate (m^3 min^{-1}), E_i is the particle emission rate in bin i (μg min^{-1}), and k_i is the loss rate constant for particles in bin i (min^{-1}). Particle losses were assumed to follow first-order decay, consistent with previous chamber-based emission studies (Wang and Chan, 2023). Following each Bakhoor burning event, particle concentrations exhibited near-exponential decay, which was used to estimate k_i by fitting the decay curves, following the approach described by Jiang et al. (2021). Emission rates were then integrated over the full burning period and summed across all size bins to obtain the total particulate emission rate.

Particle formation, growth, and early size evolution were interpreted in the context of the controlled flow-through chamber configuration. The chamber volume was 125 L and the outlet flow rate was 20 L min^{-1}, giving a dilution rate of 0.16 min^{-1}, equivalent to an air exchange rate of 9.6 h^{-1}, and a flow-through residence time of 6.25 min. Because this configuration combines a high source-to-volume ratio with flow-through dilution, the measured size distributions should not be interpreted as direct room-averaged particle concentrations or room-scale aerosol distributions. Instead, they are best viewed as controlled

near-source source-term measurements from the practical Bakhoor-on-charcoal burning configuration. Under this source-term interpretation, the measured size distributions include the outcome of near-source particle formation and early growth. For room-scale applications, these measured emission rates and size distributions can be used as source inputs, whereas subsequent evolution will depend on room volume, ventilation, mixing, deposition, surface losses, coagulation, and possible semivolatile evaporation or gas-particle repartitioning.

2.3 Ozone aging of particle samples

To simulate oxidative aging, PM-loaded filters were placed in an in-line filter holder and exposed to a continuous flow of ozone diluted in zero air. Ozone was generated by passing zero air through a mercury lamp ozone generator (Model 610, Jelight Inc., USA), and its concentration was continuously monitored at the outlet of the filter holder using an ozone analyzer (Model 106-L, 2B Technologies Inc.). Two ozone levels, approximately 200 ppb and 1500 ppb, were applied for the same 30 min duration to vary the cumulative O_3 exposure while keeping filter handling and exposure time consistent. These exposures correspond to approximately 20 h and 150 h of equivalent indoor ozone exposure, respectively, assuming a representative indoor ozone level of 5 ppb (Nazaroff and Weschler, 2022). This dose equivalence was used to approximate extended indoor O_3 exposure, while recognizing that concentration-dependent kinetics and phase partitioning may differ between accelerated and lower-concentration aging conditions. The lower exposure was selected to approximate airborne residence-scale O_3 processing, consistent with reported residential air-exchange-based particle residence times on the order of hours to about one day (Zhao and Liu, 2020; Salthammer, 2011). The higher exposure was selected to probe more extended O_3 exposure relevant to deposited indoor particle reservoirs, which can remain on indoor surfaces and undergo heterogeneous or multiphase chemical processing after removal from the airborne phase (Abbatt and Wang, 2020; Ault et al., 2020). This accelerated protocol was selected for practicality and reproducibility and to isolate ozone-driven processing under controlled conditions. Although filter-bound PM could, in principle, be exposed to lower ozone concentrations for longer periods, multi-day treatments increase the likelihood of uncontrolled changes that are not directly attributable to ozone, including slow volatilization of semi-volatile constituents, continued dark aging, and time-dependent particle-filter interactions. Using elevated ozone over short durations therefore enables consistent, well-defined oxidant doses while minimizing these confounding processes. Similar filter-based O_3 exposure of particle-loaded samples has been used previously to evaluate changes in aerosol oxidative potential, including for biomass-burning organic aerosol (Wong et al., 2019). This filter-bound O_3 treatment provides a practical approach to probe the O_3 sensitivity of Bakhoor-burning particles. O_3 was selected because it is widely regarded as an important indoor oxidant, particularly for heterogeneous and surface chemistry. It is commonly introduced indoors through air exchange, and can be delivered as a stable and controllable oxidant dose for reproducible particle-aging experiments (Waring and Wells, 2015; Weschler and Carslaw, 2018). Indoor particles may experience O_3 exposure both while airborne and after deposition onto indoor surfaces; deposited particles can persist longer and remain exposed to oxidants. Accordingly, this experiment should be interpreted as a controlled test of the post-emission O_3 responsiveness of Bakhoor-burning particle-phase material, rather than as a full simulation of suspended-particle aging in indoor air. Compared with suspended particles, filter-bound particles no longer evolve within the same gas-particle partitioning

environment, and their exposure to O_3 may be influenced by particle loading and contact with the filter substrate. In addition, indoor OH and NO_3 chemistry can occur but is more condition-dependent than the controlled O_3 exposure used here. Indoor OH can be generated through ozonolysis and photolysis-related processes, whereas NO_3 chemistry becomes more relevant under NO_2/O_3-rich conditions (Waring and Wells, 2015; Abbatt and Wang, 2020; Zannoni et al., 2022; Dewald et al., 2023). Therefore, OH- and NO_3-driven processing should be regarded as additional indoor aging pathways that were not simulated by the present filter-bound O_3 exposure and should be evaluated in future suspended-particle or mixed-oxidant studies.

2.4 Molecular characterization of organics in Bakhoor-burning particles

To analyze the molecular composition of organic species in Bakhoor-burning particles, filter samples were extracted in acetonitrile via 30-minute sonication in an ice-water bath to minimize sonication-induced heating and potential thermal degradation, followed by filtration through a 0.22 μm PTFE syringe filter. Acetonitrile was selected over methanol to minimize solvent-induced artifacts, such as the methanolysis of conjugated carbonyl species (Chen et al., 2022). The extracts were analyzed using ultra-high-performance liquid chromatography coupled with high-resolution Orbitrap mass spectrometry (UHPLC-HRMS; Orbitrap ID-X, Thermo Fisher Scientific Inc.), equipped with an electrospray ionization (ESI) source operated in positive ion mode. Chromatographic separation was performed on an Acquity HSS T3 column (1.8 μm, 2.1 mm × 100 mm; Waters Corp.) under conditions optimized for semi-polar organic compounds (Wang et al., 2021; Go et al., 2022). The liquid chromatography gradient and flow parameters were configured to improve separation efficiency and minimize matrix effects, following established protocols for analyzing dissolved organic matter and aerosol extracts (Go et al., 2022; Liang et al., 2024; Patriarca et al., 2018). Data acquisition and molecular formula assignment were conducted using Compound Discoverer software (Thermo Fisher Scientific Inc.), with elemental compositions determined from exact m/z values and isotopic patterns. This analytical workflow enabled untargeted molecular profiling of the complex organic mixtures emitted from Bakhoor burning.

2.5 Acellular dithiothreitol (DTT) assay

The oxidative potential of particulate matter is a key indicator of its capacity to generate reactive oxygen species (ROS) and induce oxidative stress (Jiang et al., 2019). Among acellular assays, the DTT assay is widely used as a proxy for particle redox activity and quantification of the rate of DTT consumption by redox-active species that catalyze electron-transfer reactions (Cho et al., 2005). The experimental protocol followed established methods reported previously (Gao et al., 2017; Fang et al., 2017; Lyu et al., 2018; Cho et al., 2005). Briefly, PM-loaded PTFE filter samples were extracted in deionized water by 30 minutes of sonication in an ice-water bath to minimize heating during extraction. Given the potential for radical formation during sonication, a comparison between sonication and vortex shaking was conducted. The results showed no significant difference in DTT consumption, indicating that sonication did not introduce measurable artifacts. The PM mass used to calculate mass-normalized DTT oxidative potential was determined gravimetrically from the difference between the pre- and post-sampling masses of the PTFE filters. For the main Bakhoor-burning and cigarette-smoke samples used in the DTT comparison, the collected PM masses varied within about a factor of four before extraction. For the measurement of water-soluble oxidative potential ($OP_{DTT,m}^{WS}$), the extract was filtered and 0.7 mL of the filtrate was mixed with 0.1 mL of 1 mM DTT

solution and 0.2 mL of potassium phosphate buffer (0.5 M, pH 7.4). The mixture was incubated at 37 °C in a thermostatic shaker with continuous agitation. At designated time points (0, 5, 10, 15, 25, and 35 minutes), 0.1 mL aliquots were withdrawn and quenched by adding trichloroacetic acid (TCA). The residual DTT in each aliquot was then reacted with Tris buffer (0.4 M containing 20 mM EDTA) and 5,5′-dithiobis-(2-nitrobenzoic acid) (DTNB). The reaction yields a yellow chromophore that absorbs at 412 nm, which was quantified using a microplate reader. The DTT consumption rate was determined from the linear decrease in residual DTT over the incubation period. To determine the total oxidative potential ($OP_{DTT,m}^{tot}$), the same procedure was used, except the extract was not filtered, and the filter itself remained in the reaction mixture. This ensured that DTT-active species associated with insoluble particles suspended in the extract or still attached to the filter surface were also included in the measurement (Fang et al., 2017; Gao et al., 2017). Blank PTFE filters processed using the same protocol were used for background correction. Because mass-normalized DTT activity can depend on particle loading and on the concentration-response behavior of the dominant DTT-active species (Charrier et al., 2016), mass-normalized DTT oxidative-potential comparisons were interpreted with this potential loading-related uncertainty in mind. However, the Chelex tests showed negligible changes in $OP_{DTT,m}^{WS}$ after metal chelation, suggesting that the specific Cu/Mn-driven mass-normalization bias reported by Charrier et al. (2016) is unlikely to dominate the source-level comparison in this study. To minimize photo-degradation of DTT and DTNB, all procedures were performed under low-light conditions by minimizing workspace lighting and covering vials with aluminum foil when not in use.

2.6 Cellular macrophage assays

Alveolar macrophages represent the first line of defense in the respiratory system and are widely used to assess oxidative and toxicological responses to PM exposure, particularly through intracellular ROS generation (Liu et al., 2023; Liu et al., 2020b; Liu et al., 2020a; Tuet et al., 2019). In this study, murine alveolar macrophages (MH-S, ATCC CRL-2019) were cultured in RPMI-1640 medium (ATCC) supplemented with 10% fetal bovine serum (FBS; VWR), 1% penicillin–streptomycin (Pen-Strep; VWR), and 50 μM β-mercaptoethanol (BME; Sigma-Aldrich). Cells were maintained at 37 °C in a humidified 5% CO_2 incubator. Prior to ROS measurements, 96-well plates were pre-coated with 10% FBS in phosphate-buffered saline (PBS) to promote cell adherence. MH-S cells were seeded at a density of 2×10^4 cells per well and incubated with the ROS-sensitive fluorescent probe carboxy-H_2DCFDA (Molecular Probes, C-400). To introduce particulate exposure, PTFE filters loaded with fresh or ozone-aged Bakhoor-burning particles or sidestream cigarette-smoke particles were directly immersed in the culture medium. A 3-minute vortex mixing step was applied to enhance dispersion of PM into the media. Cells were exposed for 24 hours, after which the filters were removed and intracellular oxidative-stress responses were measured using a microplate reader (excitation/emission: 485/525 nm). All treatments were conducted in triplicate using independent filter samples. Blank controls (media only, no PM) were used to normalize fluorescence values. Blank PTFE filter controls processed under the same immersion, vortexing, and exposure protocol were used to normalize DCFH fluorescence values. The cellular exposure experiments were designed to compare oxidative-stress responses across particle sources and aging conditions, with sidestream cigarette smoke included as a protocol-matched indoor combustion reference; no separate chemical positive control for intracellular ROS generation was included in the same exposure batch.

A mitochondrial dehydrogenase (MTT) assay was conducted to evaluate cell viability following 24-hour exposure to PM. After exposure, the culture medium in each well was replaced with 100 μL of fresh medium, and 10 μL of MTT solution (5 mg mL^{-1}) was added. Cells were incubated for an additional 4 hours at 37 °C to facilitate the formation of purple formazan crystals. Following this, 100 μL of a solubilization solution consisting of 10% SDS in 0.01 M HCl was added to each well, and incubation was continued for a further 15–18 hours under the same conditions. The absorbance at 570 nm was then measured using a microplate reader to quantify formazan formation, which serves as an indicator of mitochondrial enzymatic activity and, consequently, cell viability. A viability calibration curve was established by preparing mixtures of live and heat-inactivated (autoclaved) cells at defined ratios, treating them with the same MTT procedure, and recording their absorbance at 570 nm to relate optical density to cell survival.

3. Results and discussion

3.1 Emission characteristics of Bakhoor burning particles

Figure 1A-B show the size distributions of particle number and mass for emissions from Bakhoor burning, with smoldering sidestream cigarette smoke included as a protocol-matched indoor combustion reference. Because Bakhoor was heated on a smoldering charcoal briquette, the measured distributions reflect combined contributions from the Bakhoor material and the ignition source. A charcoal-only control is therefore included to isolate charcoal-derived emissions. In the number distribution (Figure 1A), charcoal-only burning produced a weak nucleation-mode signal largely confined to the ultrafine range, whereas Bakhoor burned on charcoal yielded substantially higher concentrations and a bimodal profile, with a dominant ultrafine mode near 30 nm and a secondary mode around 160 nm. The ultrafine-mode peak was approximately 1.4 times the secondary peak, indicating a large contribution of ultrafine particles (UFPs, <100 nm) to the total particle number. Sidestream cigarette smoke, by comparison, exhibited a unimodal number distribution centered at approximately 110 nm under the protocol used here, with a substantially lower UFP contribution. In the mass distribution (Figure 1B), Bakhoor burning produced a unimodal profile centered at approximately 350 nm, indicating that emitted mass was dominated by accumulation-mode particles. Time-resolved measurements further show that particle concentrations rose within seconds after ignition, peaked at approximately 5 min, and then decayed (Figure 1C).

Figure 1D summarizes emission rates normalized to the initial Bakhoor mass per burn and to the mass of cigarette tobacco filler consumed in the smoldering sidestream cigarette-smoke reference. On this basis, Bakhoor burning produced particle mass emission rates of 670-1690 μg min^{-1} g^{-1}, substantially higher than the same-protocol smoldering sidestream cigarette smoke reference in this study (~250 μg min^{-1} g^{-1}). The cigarette-smoke comparison was based on a controlled same-protocol smoldering condition without active puffing. Previous measurements comparing sidestream particulate matter under puffing and free-burn conditions showed that sidestream particulate matter under puffing conditions remained within approximately 0.84–0.97 times the free-burn value (Browne et al., 1980). In the context of typical indoor sources, these mass emission rates place Bakhoor burning toward the upper end of reported emission rates for activities including tobacco and incense burning, moxa, candles, and non-combustion sources such as cooking and e-cigarettes (117–3367 μg min^{-1}), while

recognizing that reported rates can vary with experimental configuration and normalization (Hu et al., 2023; Chuang et al., 2013; Jetter et al., 2002; Tian et al., 2021). Unlike conventional incense burning, however, Bakhoor combines a charcoal ignition source with a chemically complex mixture of perfumed wood and additives. Number-based emission rates for Bakhoor reached (6-7)×10^{11} particles min^{-1} g^{-1}, with UFPs accounting for 70–75% of total number, compared with ~47% for the smoldering cigarette-smoke reference. Taken together, these results identify Bakhoor burning as a high-intensity indoor particle source that is strongly enriched in UFPs by number while also producing substantial fine-particle mass emissions. Because Bakhoor burning generated high particle number concentrations in the chamber, particle-particle coagulation may contribute to the evolution of the measured size distribution. To evaluate its potential influence under our experimental conditions, representative same-size Brownian coagulation kernels were calculated for 20 and 100 nm particles using the Fuchs transition-regime formulation. The estimated kernels were $2.35 \times 10^{-9}$and 1.43×10^{-9} cm^3 s^{-1}, respectively (Hinds and Zhu, 2022; Seinfeld and Pandis, 2016). With the burning-period-averaged UFP number concentration of approximately 1.0×10^6 cm^{-3}, these kernels correspond to coagulation timescales of approximately 7.1 and 11.6 min for 20 and 100 nm particles, respectively. These values are comparable to or longer than the chamber flow-through residence time of 6.25 min, suggesting that coagulation may influence the smaller end of the UFP mode but is unlikely to dominate the burning-period-averaged particle number estimate. Since coagulation reduces particle number and shifts particles toward larger diameters, the reported UFP number emission rates may represent conservative estimates.

3.2 The potential drivers of particle formation during Bakhoor burning

Figure 2A shows that charcoal-only burning produces a short-lived nucleation-mode signal immediately after ignition that decays rapidly, whereas Bakhoor burning sustains elevated particle concentrations and extends to larger particle diameters. This side-by-side comparison was conducted under the same chamber flow-through configuration and indicates that the sustained particle formation observed during Bakhoor burning cannot be explained by the charcoal ignition source alone. Instead, it is consistent with additional particle-forming material released from Bakhoor. To identify the Bakhoor components responsible for this behavior, Bakhoor materials were operationally separated into the hexane-soluble fraction (HSF) and the wood residue. The HSF is a solvent-defined operational fraction containing hexane-soluble organic material, which may include fragrance oils, resins, and related additives. The residue represents the nonextractable wood matrix. Burning the corresponding wood residues yielded nearly identical particle mass emission rates across the three Bakhoor types, whereas the original Bakhoor materials varied by approximately 2.5-fold in mass emission rates (Figure 2B). This contrast indicates that the observed differences among commercial products are primarily driven by the HSF rather than by the base wood substrate under the conditions used here. Because solvent extraction could, in principle, alter the physical structure of the remaining wood residue and independently influence combustion behavior, we conducted a reconstitution experiment as a functional control. In this experiment, the extracted HSF was recombined with the corresponding wood residue at the appropriate mass fractions and burned under the same conditions. The reconstituted material reproduced particle mass emission rates similar to those of the original samples (Figure S3), suggesting that extraction-induced changes to the residual wood matrix did not

dominate the observed emission differences. We therefore interpret the HSF as an operationally defined fraction that plays a major role in particle formation during Bakhoor burning.

Across the original Bakhoor samples, the HSF loading (9-22% by mass) was strongly associated with particle mass emissions (Figure 2B), with Type 2 exhibiting both the highest HSF loading and the highest mass emission rate. Perturbation experiments that partially reduced the HSF (tissue wiping) and increased it by recombining the HSF with the wood residue collapsed onto a common relationship between emission rate and HSF loading across all Bakhoor types. This relationship supports HSF loading as the primary control on emission magnitude, even though the composition of the HSF varied slightly among samples (Figure S4). This dependence was well described by a power-law relationship ($\beta \approx 2.1$; Figure 2B), demonstrating a nonlinear response in which emissions increase more steeply as the HSF increases. Adding HSF to reach approximately 10 wt % of the reconstructed material increased mass emission rates by ~1.7-fold, whereas increasing the HSF content to approximately 20 wt % increased emissions by ~4.3-fold. This pattern suggests a threshold-like increase in effective particle formation efficiency, where incremental increases in available precursors result in disproportionate increases in particle production (Zhang et al., 2010).

Thermogravimetric analysis (TGA) was used to assess whether the observed HSF dependence could be primarily explained by simple evaporation of intact additives. Across the three Bakhoor types, thermograms were similar and showed only minor mass loss (approximately 5%) below 100-120 °C (Figure S5), whereas most mass loss occurred between approximately 150 and 350 °C. Thermocouple measurements showed that the charcoal temperature reached approximately 300 °C within 15 s of sustained ignition in our setup (Figure S6), suggesting that Bakhoor materials are quickly driven into a higher-temperature regime rather than remaining in a low-temperature evaporation window. The reported onset of wood pyrolysis (approximately 180 °C) refers primarily to the lignocellulosic wood substrate (Escalante et al., 2022). In contrast, the HSF consists of nonstructural, solvent-extractable organics introduced during product formulation, which may volatilize and thermally transform over overlapping temperature windows during heating on charcoal. Taken together, these results suggest that HSF-linked particle formation is not solely explained by low-temperature evaporation and likely involves thermochemical processing during heating that generates condensable products, as illustrated in Figure 2C. Because TGA does not provide a mass balance for emitted particles, it is used here to bracket plausible precursor-generation regimes rather than to quantify particle yields.

3.3 Oxidative potential of particles from Bakhoor burning

To evaluate the oxidative potential of particles emitted from Bakhoor burning, we applied the dithiothreitol (DTT) assay. We report the particle mass-normalized DTT oxidative potential for both filtered aqueous extracts ($OP_{DTT,m}^{WS}$, pmol min^{-1} μg^{-1}) and total unfiltered aqueous suspensions ($OP_{DTT,m}^{tot}$, pmol min^{-1} μg^{-1}) to gauge the relative contributions of water-soluble versus suspension-associated components. Fresh Bakhoor water extracts exhibited an average $OP_{DTT,m}^{WS}$ of approximately 32 pmol min^{-1} μg^{-1} (Figure 3A). This value was not corrected by subtracting the charcoal-only burn and therefore represents the exposure-relevant oxidative potential of the full particle mixture emitted under the common real-use scenario in which Bakhoor

is heated on smoldering charcoal. This magnitude lies within reported ranges for laboratory-generated particles from indoor combustion sources (8-95 pmol min^{-1} μg^{-1}; Hu et al., 2023; Zhang et al., 2024) and for raw wood/biomass materials such as pine (35-117 pmol min^{-1} μg^{-1}; Zhang et al., 2024), and is comparable to values reported for ambient PM and biomass-burning organic aerosol fractions. Notably, the $OP_{DTT,m}^{WS}$ of Bakhoor burning particles exceeds the typical range for wildfire-influenced PM (2-16 pmol min^{-1} μg^{-1}; Fang et al., 2023), reaching values near the upper end of the wildfire range (around 32 pmol min^{-1} μg^{-1}; Isenor et al., 2025). Under the same assay conditions, cigarette smoke particles showed a higher $OP_{DTT,m}^{WS}$ of approximately 50 pmol min^{-1} μg^{-1}, about 40% higher than Bakhoor burning particles. To assess the contribution of insoluble components, $OP_{DTT,m}^{tot}$ was also measured for total particle suspensions (Fang et al., 2023; Charrier and Anastasio, 2012; Brehmer et al., 2019). Only a modest enhancement (approximately 10%) was observed relative to filtered extracts (Figure 3A), suggesting that DTT-reactive species are captured predominantly in the aqueous phase under the extraction conditions used here.

Oxidative aging can further shape exposure-relevant redox properties because indoor oxidants can transform particle composition and, in turn, DTT consumption (Wong et al., 2019; Wang et al., 2023). Following the O_3-aging protocol described in Section 2.3, we evaluate here how controlled O_3 exposure alters the oxidative potential of Bakhoor-burning and cigarette-smoke particles. Residential air exchange rates typically range from 0.05 to 1 h^{-1} (Zhao and Liu, 2020; Salthammer, 2011), corresponding to ventilation-based particle residence times of approximately 1-20 h. Moreover, the high indoor surface-to-volume ratio promotes rapid particle deposition to surfaces (Abbatt and Wang, 2020), creating surface reservoirs that are not removed by ventilation and can persist for days. These deposited materials can continue to undergo chemical processing on indoor surfaces and may remain relevant to exposure if later disturbed or transferred by human activity, air movement, or cleaning. After an ozone dose equivalent to approximately 150 h at an indoor ozone level of 5 ppb (Figure 3B), $OP_{DTT,m}^{WS}$ increased by approximately 15% for both Bakhoor and cigarette smoke particles. This increase suggests the net formation of more DTT-active oxygenated products during ozonolysis, consistent with a rise in the carbon oxidation state (OSc) derived from mass spectrometric analysis (Figures S7 and S8). Across fresh and O_3-aged samples, the median $OP_{DTT,m}^{WS}$ of Bakhoor water extracts fell within the broad range reported for laboratory combustion-derived PM and overlapped values reported for field PM (Figure 3C), although many field studies report total $OP_{DTT,m}^{tot}$, which is typically higher than the water-soluble fraction. Prior work by Wong et al. (2019) reported an initial increase in DTT activity (~20%) during the early stages of ozonolysis of biomass-burning particles, followed by a decrease toward baseline after extended aging (up to 70 h), suggesting that some DTT-active products can be transient. Quinone-like redox-cycling species, which catalyze ROS formation, have been proposed as plausible contributors to the observed changes in oxidative potential (Xiong et al., 2017). These observations motivate identifying the chemical drivers that govern DTT consumption in Bakhoor smoke.

3.4 Potential chemical contributors to DTT activity

To examine which particle-phase constituents may underlie the observed DTT response, we analyzed extracts of Bakhoor burning and cigarette smoke particles using UHPLC-HRMS. Both sources showed broad distributions of detected features

spanning *m/z* ≈ 100-400 (Figure S9), consistent with LC/ESI-MS characterizations of biomass-burning organic aerosol and combustion-derived organic aerosol (Smith et al., 2009). Despite comparable *m/z* envelopes, the assigned elemental-composition classes differed markedly between the two sources. Bakhoor burning particles were dominated by CHO formulas (~65% of assigned species), whereas cigarette smoke particles were relatively less oxygenated and strongly enriched in nitrogen-containing formulas (CHN+CHON≈84%) (Figure S9). These comparisons were based on relative ESI+ feature intensities, calculated as the signal contribution of each assigned feature normalized to the total assigned ESI+ signal within the same sample. This normalization emphasizes differences in the distribution of detected molecular features between Bakhoor-burning and cigarette-smoke particles, rather than differences in total extracted signal or absolute ion abundance. Because all samples were analyzed using the same extraction, chromatographic, ionization, and data-processing workflow, the observed contrast provides an internally consistent ESI+-resolved source fingerprint comparison. Electrospray ionization polarity is analyte-dependent, and positive and negative modes provide complementary molecular coverage (Liigand et al., 2017; Patriarca et al., 2018). Therefore, the stronger CHN/CHON contribution detected in cigarette smoke may reflect both real source differences and favorable ESI+ response of nitrogen-containing compounds, while acidic or highly oxygenated CHO species may be less efficiently represented under ESI+ conditions. Accordingly, these molecular patterns should be interpreted as ESI+-resolved source fingerprints rather than a complete quantitative inventory of particle-phase organics. Since elemental class alone provides limited insight into structural motifs relevant to redox cycling, we also computed the modified aromaticity index (AI_{mod}, see Text S1 for details) as a proxy for unsaturation and aromatic character and classified formulas as aromatic ($AI_{mod} \geq 0.5$), olefinic ($0 < AI_{mod} < 0.5$), or aliphatic ($AI_{mod} = 0$) (Koch and Dittmar, 2006; Song et al., 2021; Song et al., 2019).

We then related $OP_{DTT,m}^{WS}$ to molecular-formula-derived metrics (AI_{mod}, O:C, N:C) across fresh and ozone-aged samples from both sources (Figure 4). Across the full dataset, aromatic-like formulas ($AI_{mod} \geq 0.5$) exhibited the strongest positive association with $OP_{DTT,m}^{WS}$ (R^2>0.5). The strongest correlations were observed for moderately oxygenated formulas (O:C ≈ 0.05-0.15), indicating that the DTT response likely tracks most closely with unsaturated/aromatic-like formulas and is consistent with the O:C range often associated with redox-active aromatic products, including quinone-like structures (Charrier and Anastasio, 2012). In contrast, highly oxidized formulas (e.g., acid-rich CHO species at higher O:C) and aliphatic-like formulas ($AI_{mod} = 0$) showed weaker associations with $OP_{DTT,m}^{WS}$ (Shultz et al., 2011; Park et al., 2006). These interpretations are based on molecular formulas and bulk metrics. Definitive assignment to specific compound classes (e.g., individual quinones) requires targeted identification and standards.

Nitrogen-containing aromatic-like formulas also exhibited positive associations with $OP_{DTT,m}^{WS}$, with the strongest relationships observed at N:C≈0.10-0.25. Because the strongest correlations overall occurred for aromatic-like formulas with high AI_{mod}, this pattern suggests that nitrogen substitution within unsaturated/aromatic-like structures may mark an additional set of formulas associated with DTT activity at the molecular-formula level. The intrinsic DTT reactivity of individual nitrogen-containing organics remains less well constrained than that of quinone-type species, but prior work has linked

nitroaromatics and N-heterocycles to enhanced DTT responses in complex mixtures (Lai et al., 2025). Nitrogen functionalities may also influence redox cycling indirectly, for example by modulating electron density or stabilizing redox intermediates in mixed organic matrices (Dou et al., 2015). Consistent with these ESI+ resolved source fingerprints, Bakhoor-burning particles were dominated by CHO formulas and only a minority met the aromatic-like criterion ($AI_{mod} \geq 0.5$; Figure S11), whereas a substantially larger fraction of cigarette-derived CHN/CHON formulas were aromatic-like (Figure S11). Within the ESI+ molecular feature space, this pattern is consistent with the higher $OP_{DTT,m}^{WS}$ observed for cigarette-smoke particles and with the positive association between $OP_{DTT,m}^{WS}$ and ESI+ detected nitrogen-containing aromatic-like formulas. However, these correlations are interpreted as empirical structure–activity associations within the measured ESI+ molecular feature space, rather than as quantitative apportionment of the full particle-phase organic mixture or as evidence for the absence of redox-active species outside this analytical window.

Finally, since dissolved transition metals can contribute to DTT activity directly and/or via interactions with organics (Jiang et al., 2019; Wang et al., 2018b), we conducted metal-chelation tests using Chelex resin. $OP_{DTT,m}^{WS}$ changed negligibly after chelation (Figure S12), indicating a minimal contribution from dissolved metals and suggesting that $OP_{DTT,m}^{WS}$ in both sources is dominated by organic species.

3.5 Cellular oxidative-stress responses induced by Bakhoor burning particles

To further assess cellular oxidative-stress responses to Bakhoor burning particles, we quantified intracellular fluorescence signals in alveolar macrophages using a DCFH-based assay and reported responses as fold changes relative to untreated controls. This cellular endpoint complements the acellular DTT assay by capturing integrated intracellular oxidant signaling under particle exposure. As described in the Methods, five particle dose levels were tested for each sample, dose-response relationships were fitted using the Hill equation, and the area under the fitted dose-response curve (AUC) was used as an integrative metric to quantify the overall oxidative response (Figure 5A) (Tuet et al., 2016).

Bakhoor burning particles elicited stronger DCFH fluorescence responses than sidestream cigarette smoke particles across the tested dose range (Figure 5B). The AUC metric ranged from 0.51 to 0.62 for Bakhoor samples, higher than 0.41 for cigarette smoke. Naphthalene-derived SOA was used as an external cellular-response reference because it is a well-studied anthropogenic aromatic SOA system that has been shown to induce strong macrophage DCFH responses under a comparable assay framework (Tuet et al., 2017). The magnitude of the response induced by Bakhoor burning particles was comparable to that reported for naphthalene-derived secondary organic aerosol. At higher particle doses, the fluorescence response approached a plateau (Figure 5A), consistent with saturation of the assay response and/or the onset of cytotoxicity, as supported by the accompanying MTT viability results (Figure S13). Because high particle doses can reduce cell viability, DCFH fluorescence at the upper end of the dose-response curve may include contributions from cytotoxicity-associated processes. We therefore used the MTT assay to define a non-cytotoxic low-dose range, with cell viability greater than 80% of the untreated control as a conservative criterion. This threshold is stricter than the 70% viability cutoff commonly used in ISO 10993-5-based cytotoxicity assessment (International Organization for Standardization, 2009). The three lowest loading levels, 0.0001×,

0.001×, and 0.01×, were selected for the low-dose AUC analysis. The DCFH AUC over this range was calculated using baseline-subtracted DCFH fold changes. Because this range included three dose points, trapezoidal integration over log10-transformed particle loading was used. For fresh total-particle samples, the low-dose AUC values for the three Bakhoor samples were 0.249, 0.241, and 0.215, compared with 0.140 for the protocol-matched sidestream cigarette-smoke reference. These results indicate that Bakhoor-burning particles induced measurable intracellular oxidative-stress responses under low-dose exposure conditions before substantial viability loss. The higher-dose responses were retained as part of the full dose-response characterization but were interpreted in light of the MTT viability results. MTT viability further showed a dose-dependent reduction in cellular metabolic activity at higher particle mass loadings (Figure S13). Cell viability was largely maintained at the lower loadings used for the low-dose DCFH AUC analysis, whereas higher loadings led to a marked reduction in viability. This result supports the interpretation that DCFH responses in the low-dose range occurred before substantial viability loss, whereas responses at higher loadings may be influenced by reduced cellular metabolic activity. Such combined interpretation of acellular oxidative potential, intracellular oxidative-stress response, and MTT-based cytotoxicity is consistent with prior PM toxicology studies using complementary chemical and cellular endpoints (Lionetto et al., 2021). An additional consideration for the macrophage assay is the potential contribution of endotoxin, because lipopolysaccharide can activate macrophage inflammatory and ROS-related responses (Sanlioglu et al., 2001; Maitra et al., 2009). Endotoxin-specific quantification, such as the Limulus amebocyte lysate assay or recombinant Factor C analysis (Lee et al., 2004), was not included in this study. However, the cells were exposed to particles emitted from Bakhoor heated on smoldering charcoal, rather than to raw wood or botanical materials directly suspended in culture medium. Dry-heat treatment at 170–250 °C has been shown to reduce lipopolysaccharide activity (Tsuji and Harrison, 1978). In our setup, the charcoal temperature reached approximately 300 °C (Figure S6), and this high-temperature processing may have reduced potential contributions from raw-material-associated endotoxin. Residual particle-associated endotoxin nevertheless cannot be fully excluded without endotoxin-specific quantification. If such material remained associated with the emitted particles, it would be part of the particle mixture generated under the real-use Bakhoor-burning condition, rather than an external contaminant introduced during sample handling. The absence of endotoxin-specific quantification mainly limits detailed attribution of the macrophage response drivers, rather than the observation that Bakhoor-burning particles induced a DCFH response under the exposure protocol used here.

Notably, these cellular oxidative-stress responses differed from the acellular DTT results, for which cigarette smoke particles exhibited 47-100% higher $OP_{DTT,m}^{WS}$ than Bakhoor burning particles. Such divergence is expected because DTT and DCFH-based cellular readouts probe different chemical and biological processes and can be weakly correlated for complex mixtures (Kim et al., 2014; Tuet et al., 2016; Seo et al., 2025). Similar assay-dependent discrepancies have been reported previously; for example, Tuet et al. (2016) observed weak or absent correlations between DTT activity and DCFH-based cellular oxidative-stress responses for some wintertime ambient PM samples. Mechanistically, DTT primarily reflects the electron-transfer capacity of extractable species in a simplified buffer system, whereas the cellular assay integrates particle delivery and uptake, intracellular bioactivation, depletion of redox buffers, and activation of oxidant-generating pathways

(Kim et al., 2014). Collectively, these results underscore that DTT alone may not capture the full spectrum of oxidative-stress potential for indoor combustion aerosols.

Although mechanistic attribution of cellular signaling to specific molecules is inherently challenging, the compositional information provides plausible hypotheses for why Bakhoor burning particles produced stronger cellular oxidative-stress responses. Bakhoor extracts were enriched in oxygenated CHO formulas (Figures S9 and S10), consistent with a larger contribution from oxygenated organics, some of which may contain electrophilic carbonyl functionality. Electrophilic aldehydes and related carbonyls are well known to form covalent adducts with cellular nucleophiles, particularly cysteine thiols in glutathione and proteins, thereby depleting intracellular thiol buffering capacity and perturbing redox homeostasis in ways that can amplify downstream oxidant signaling (Fritz and Petersen, 2013; Lopachin and Gavin, 2014). AI_{mod} classification further places a substantial fraction of Bakhoor CHO formulas in the olefinic and non-aromatic unsaturated regimes (Figure S11). These less-condensed CHO structures may be more conformationally flexible than condensed aromatic frameworks and may interact differently with lipid phases, potentially affecting cellular delivery and subsequent bioactivation (Liu et al., 2011). By contrast, cigarette smoke particles were enriched in nitrogen-containing formulas (CHN/CHON, Figure S11) yet produced a lower net DCFH response under the exposure conditions used here, suggesting that the dominant chemical drivers of $OP_{DTT,m}^{WS}$ and cellular oxidative-stress responses differ across sources.

4. Atmospheric implications

This study demonstrates that Bakhoor burning is a potent indoor source of fine particles, particularly with a substantial ultrafine fraction. Across the three products tested here, Bakhoor burning produced particle mass and number emission rates of 670-1690 μg min^{-1} g^{-1} and (6-7) × 10^{11} particles min^{-1} g^{-1}, respectively, with ultrafine particles accounting for 70-75 % of total particle number. On a mass-normalized basis, these emission rates were approximately 4.3-fold higher than those of the protocol-matched smoldering sidestream cigarette-smoke reference. Together with the observed size distributions, these results indicate that routine Bakhoor use can generate exposure-relevant particle burdens comparable to, and in some use scenarios exceeding, those from more widely recognized indoor combustion sources. Because respiratory deposition varies strongly with particle diameter and differs between the tracheobronchial (Tb) and alveolar (Al) regions (Figures 6A and 6B), lung-deposited surface area (LDSA; see Text S2) was estimated as an inhalation-relevant dose metric that has been shown to track inflammatory and cytotoxic responses across particle types more consistently than particle mass alone (Hofmann, 2011; Oh et al., 2023). Using the mean emission factors measured here together with size-resolved regional deposition fractions from Hofmann (2011), the Bakhoor-to-cigarette LDSA ratio exhibits strong size dependence and reaches its highest values in the ultrafine range (Figure 6B). Because particles at intermediate diameters dominate the emitted size distribution and the integrated surface-area dose (Figure S14), the LDSA ratio integrated over the measured size range is approximately 4 for both the Tb and Al regions (Figure 6C). This LDSA calculation assumes spherical particles when converting measured size distributions to particle surface area. It should be noted that nonspherical or agglomerated combustion particles may introduce a morphology-dependent surface-area uncertainty (Decarlo et al., 2004; Ku and Maynard, 2005; Levin et al., 2016). For a

reported Bakhoor use rate of 0.4-2.9 g d^{-1} (Bu-Olayan and Thomas, 2021), this scaling suggests that the daily inhalation-relevant dose from Bakhoor burning may be comparable to that from multiple cigarettes of smoldering sidestream smoke under the reference condition used here, although the real-world equivalence will vary with room volume, ventilation, and burning practice.

Across the samples tested here, the combination of acellular DTT activity and macrophage DCFH responses shows that Bakhoor burning particles exhibit substantial oxidative potential and cellular oxidative-stress responses. Relative to sidestream cigarette smoke particles, these responses differ between assays on a per-mass basis and persist after ozone aging over multi-day equivalent exposures. Fresh Bakhoor extracts showed an average $OP_{DTT,m}^{WS}$ of approximately 32 pmol min^{-1} μg^{-1}, ozone aging increased $OP_{DTT,m}^{WS}$ by about 15 % under the conditions used here, and the DCFH-based AUC values for Bakhoor samples ranged from 0.51 to 0.62, compared with 0.41 for the sidestream cigarette-smoke reference. These results suggest that the oxidative properties of Bakhoor-burning particles can remain relevant after post-emission aging, rather than being limited to freshly emitted particles alone. This may be particularly important in indoor environments with limited ventilation and repeated daily use, where particle accumulation and continued chemical processing by indoor oxidants and surface interactions may extend the relevance of these responses beyond the point of emission. Such conditions are especially relevant in hot-arid regions such as the Middle East, where indoor spaces are frequently cooled using air-conditioning systems and windows may remain closed; in many settings with limited outdoor-air supply, air-exchange rates can be low (for example, <0.5 h^{-1}) (Indraganti et al., 2016; Diapouli et al., 2013). The accompanying reduction in cell viability further suggests that these oxidative responses may be associated with measurable biological effects under the in vitro exposure conditions tested here. Relating these in vitro exposure conditions to human lung dose, however, will require dedicated dosimetry and exposure modeling and should be addressed in future work.

The control and perturbation experiments further identify the hexane-soluble fraction (HSF) as an important leverage point for particle formation during Bakhoor burning. Operational treatments that reduced the HSF, including solvent extraction to generate wood residue and a simple tissue-wiping step to partially remove surface-associated HSF, lowered particle mass emissions. However, these perturbations yielded slightly higher particle mass-normalized DTT oxidative potential relative to untreated material (Figure S15), indicating that emission reductions do not necessarily lead to a reduction in oxidative potential on a mass basis. Nevertheless, when mass-normalized DTT oxidative potential is combined with the corresponding emission factors to estimate emission-weighted total DTT consumption, the net oxidative burden decreases for the HSF-reduced treatments (Figure S15). These results indicate that the HSF strongly influences both emission magnitude and oxidative properties. Because HSF loading varies across products, lowering HSF loading may provide a practical pathway to reduce emitted particle mass and, consequently, exposure, although hazard-relevant endpoints should be evaluated in parallel rather than inferred from emissions alone. At the user level, wiping Bakhoor pieces prior to burning may partially remove surface-associated HSF and reduce emissions, although the extent of emission reduction will likely depend on product composition and user practice and should be evaluated under realistic operating conditions. Electric Bakhoor burners may also represent a useful alternative by eliminating charcoal-assisted combustion and potentially reducing combustion-related particle formation,

but their net effects on emissions and toxicity require evaluation under realistic use conditions before broad recommendations can be made. More broadly, these results identify source composition and burning configuration as important controls on particle emissions from Bakhoor burning, while highlighting the additional role of ventilation in shaping real-use exposure.

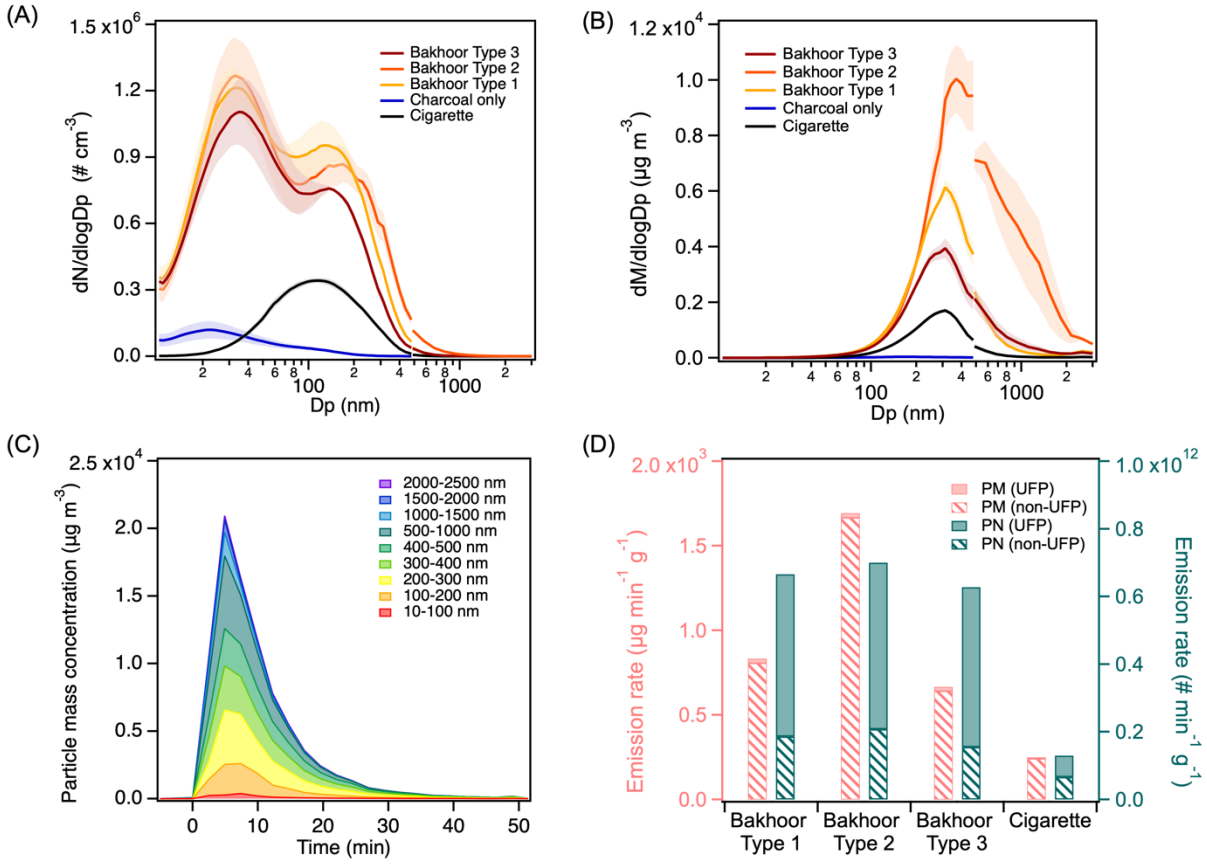

Figure 1. (A) Number and (B) mass size distributions measured in the chamber during Bakhoor burning on charcoal (three products) and smoldering sidestream cigarette smoke, with a charcoal-only control; distributions are shown without size-dependent loss correction. (C) Average particle mass concentration as a function of time following Bakhoor burning, resolved by particle size ranges and shown without loss correction. (D) Particle emission rates, with mass (left axis) and number (right axis) normalized to the initial Bakhoor mass per burn and to the mass of cigarette tobacco filler, respectively, reported separately for ultrafine and non-ultrafine size fractions and corrected for size-dependent losses. The apparent discontinuity near 500 nm in panels A and B reflects the use of two instruments: particles below 500 nm were measured by the SEMS, whereas particles above 500 nm were measured by the OPC. This discontinuity is therefore not interpreted as a physical feature of the emitted aerosol size distribution.

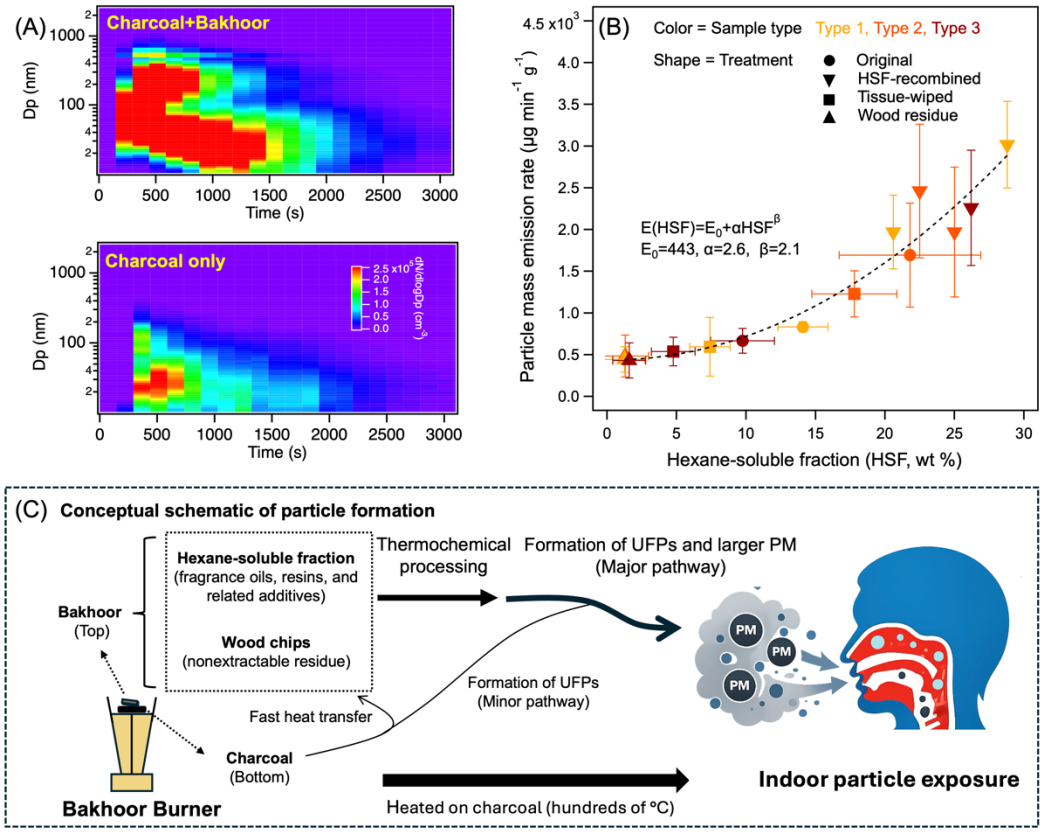

555

556 **Figure 2.** (A) Time-resolved particle number size distributions ($dN/dlogD_p$) measured during Bakhoor burning (with charcoal
557 used for ignition) and during a charcoal-only control, shown as contour maps of mobility diameter (D_p) versus time. (B) Particle
558 mass emission rate as a function of the loading of the hexane-soluble fraction (HSF, wt %) in Bakhoor materials. Colors denote
559 Bakhoor type, and symbols denote treatment (original, HSF-recombined, tissue-wiped, and wood residue). The dashed curve
560 shows an empirical fit, $E(HSF) = E_0 + \alpha HSF^{\beta}$ (parameters shown). (C) Conceptual schematic linking Bakhoor composition
561 and heating on charcoal to fine particle formation and indoor particle exposure.

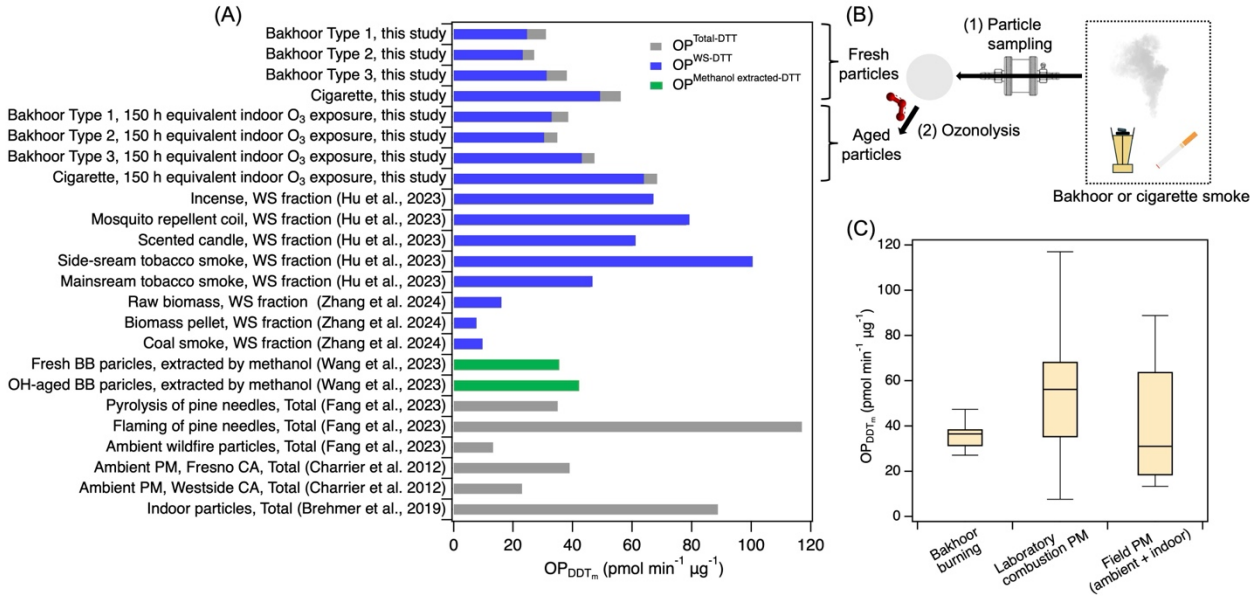

Figure 3. (A) The mass-normalized DTT consumption rate (OP_{DTTm}) for Bakhoor burning and sidestream cigarette smoke particles in this study (fresh and ozone-aged), shown alongside literature values for other laboratory combustion aerosols and field PM. (B) Schematic of particle collection on filters and subsequent ozonolysis of PM-loaded filters prior to DTT analysis. (C) Box plot summarizing OP_{DTTm} grouped as Bakhoor burning, other laboratory combustion PM and field PM.

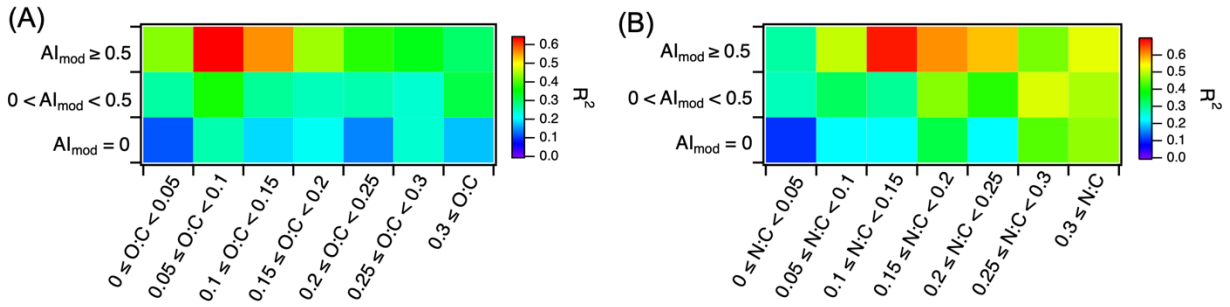

Figure 4. Heat maps of the coefficient of determination (R^2) from linear regressions relating the water-soluble mass-normalized DTT oxidative potential ($OP^{WS}_{DTT,m}$) to the summed UHPLC–HRMS signal intensity of molecular-formula bins grouped by modified aromaticity index (AI_{mod}) and (A) oxygen-to-carbon (O:C) or (B) nitrogen-to-carbon (N:C) ratio, across fresh and ozone-aged Bakhoor burning and cigarette smoke samples.

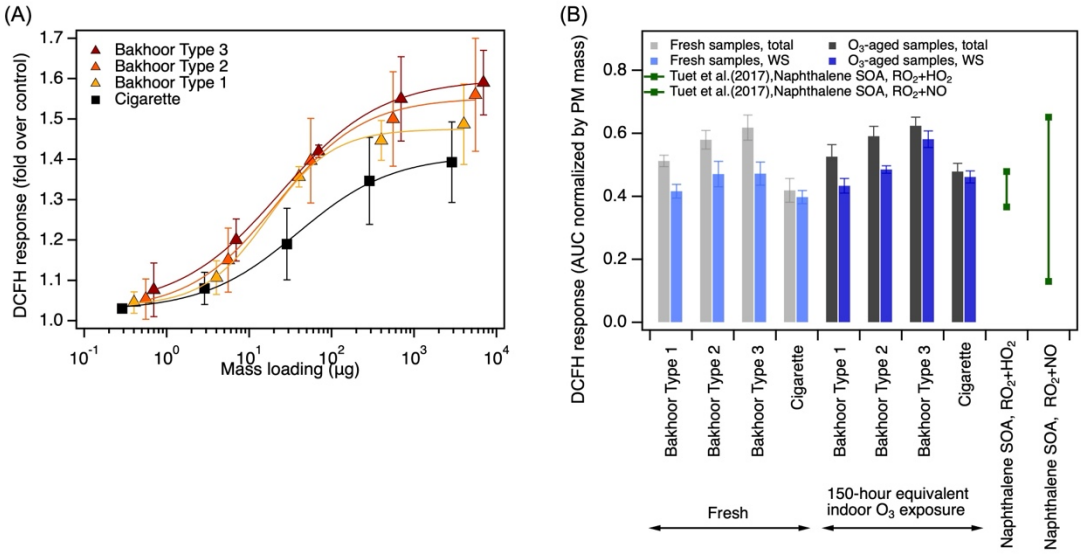

Figure 5. Intracellular oxidative-stress responses (DCFH assay) induced by particles from three Bakhoor types and sidestream cigarette smoke. (A) Dose–response curves of DCFH fluorescence (reported as fold change relative to untreated controls) as a function of particle mass loading; solid lines denote Hill-equation fits. (B) Integrated responses quantified as the area under the fitted dose–response curve (AUC), normalized by particle mass, for fresh and O_3-aged samples and for total particle suspensions and water-soluble (WS) extracts. Reference values for naphthalene SOA are from Tuet et al. (2017).

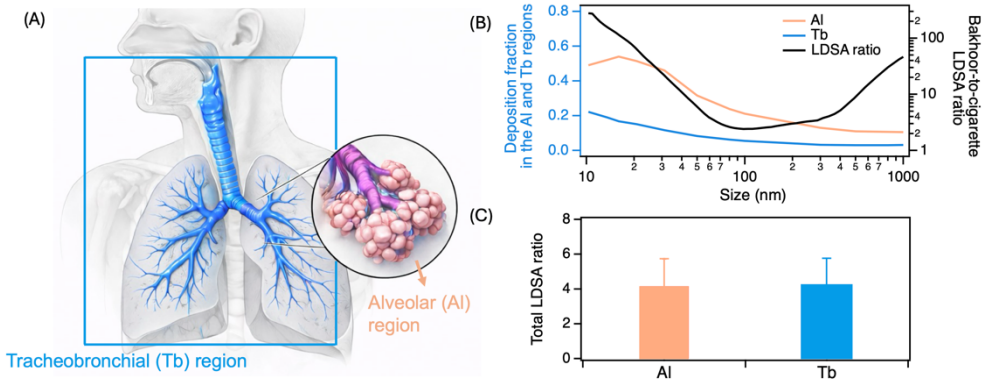

Figure 6. (A) Schematic of the human respiratory tract highlighting the tracheobronchial (Tb) and alveolar (Al) regions used for deposition calculations. (B) Size-resolved regional deposition fractions for the Tb and Al regions (left axis) and the corresponding size-resolved ratio of lung-deposited surface area (LDSA) for Bakhoor burning particles relative to sidestream cigarette smoke particles (right axis). (C) Bakhoor-to-cigarette LDSA ratio integrated over the measured particle size range for the Tb and Al regions; error bars denote ±1 standard deviation (1σ).

Data availability. All datasets used in this study, as well as the data products generated during the analysis, are available from the corresponding author upon request. These data are not publicly archived because they are maintained as multiple processed and analysis-specific files rather than as a repository-ready dataset.

Author contributions. CKC and LZ designed the experiment; LZ and ZL conducted the experiments; LZ, ZL and WX performed the data interpretation; LZ, ZL, WX, RJH and CKC wrote the paper. All authors contributed to the paper with useful scientific discussions or comments.

Competing interests. The contact author has declared that neither they nor their co-authors have any competing interests.

Acknowledgements. C.K.C. gratefully acknowledges support from the KAUST Baseline Research Fund (BAS/1/1432-01-01), the Center of Excellence for Smart Health (KCSH) Fund (award no. 5932) at King Abdullah University of Science and Technology, and the Hong Kong Research Grants Council (11304121 and 11314222).

References

Abbatt, J. P. D. and Wang, C.: The atmospheric chemistry of indoor environments, *Environmental Science: Processes & Impacts*, **22**, 25–48, 2020.

Alarifi, S. A., Mubarak, M. M., and Alokail, M. S.: Ultrastructural changes of pneumocytes of rat exposed to Arabian incense (Bakhour), *Saudi Medical Journal*, **25**, 1689–1693, 2004.

Brehmer, C., Lai, A., Clark, S., Shan, M., Ni, K., et al.: The oxidative potential of personal and household PM2.5 in a rural setting in southwestern China, *Environmental Science & Technology*, **53**, 2788–2798, 2019.

Bu-Olayan, A. H. and Thomas, B. V.: Exposition of respiratory ailments from trace metals concentrations in incenses, *Scientific Reports*, **11**, 10210, https://doi.org/10.1038/s41598-021-89493-w, 2021.

Charrier, J. G. and Anastasio, C.: On dithiothreitol (DTT) as a measure of oxidative potential for ambient particles: Evidence for the importance of soluble transition metals, *Atmospheric Chemistry and Physics*, **12**, 11317–11350, 2012.

Chen, C. and Zhao, B.: Indoor emissions contributed the majority of ultrafine particles in Chinese urban residences, *Environmental Science & Technology*, **58**, 8444–8456, https://doi.org/10.1021/acs.est.4c00556, 2024.

Chen, K., Raeofy, N., Lum, M., Mayorga, R., Woods, M., et al.: Solvent effects on chemical composition and optical properties of extracted secondary brown carbon constituents, *Aerosol Science and Technology*, **56**, 917–930, 2022.

Cho, A. K., Sioutas, C., Miguel, A. H., Kumagai, Y., Schmitz, D. A., et al.: Redox activity of airborne particulate matter at different sites in the Los Angeles Basin, *Environmental Research*, **99**, 40–47, 2005.

Chuang, H.-C., BéruBé, K., Lung, S.-C. C., Bai, K.-J., and Jones, T.: Investigation into the oxidative potential generated by the formation of particulate matter from incense combustion, *Journal of Hazardous Materials*, **244–245**, 142–150, https://doi.org/10.1016/j.jhazmat.2012.11.034, 2013.

Cincinelli, A. and Martellini, T.: Indoor air quality and health, *International Journal of Environmental Research and Public Health*, **14**, 1286, 2017.

Dalibalta, S., Elsayed, Y., Alqtaishat, F., Gomes, I., and Fernandes, N.: A health risk assessment of Arabian incense (Bakhour) smoke in the United Arab Emirates, *Science of The Total Environment*, **511**, 684–691, https://doi.org/10.1016/j.scitotenv.2014.12.024, 2015.

Diapouli, E., Chaloulakou, A., and Koutrakis, P.: Estimating the concentration of indoor particles of outdoor origin: A review, *Journal of the Air & Waste Management Association*, **63**, 1113–1129, 2013.

Dou, J., Lin, P., Kuang, B.-Y., and Yu, J. Z.: Reactive oxygen species production mediated by humic-like substances in atmospheric aerosols: Enhancement effects by pyridine, imidazole, and their derivatives, *Environmental Science & Technology*, **49**, 6457–6465, https://doi.org/10.1021/es5059378, 2015.

Elsayed, Y., Dalibalta, S., Gomes, I., Fernandes, N., and Alqtaishat, F.: Chemical composition and potential health risks of raw Arabian incense (Bakhour), *Journal of Saudi Chemical Society*, **20**, 465–473, 2016.

Escalante, J., Chen, W.-H., Tabatabaei, M., Hoang, A. T., Kwon, E. E., et al.: Pyrolysis of lignocellulosic, algal, plastic, and other biomass wastes for biofuel production and circular bioeconomy: A review of thermogravimetric analysis (TGA) approach, *Renewable and Sustainable Energy Reviews*, **169**, 112914, 2022.

Fang, T., Zeng, L., Gao, D., Verma, V., Stefaniak, A. B., et al.: Ambient size distributions and lung deposition of aerosol dithiothreitol-measured oxidative potential: Contrast between soluble and insoluble particles, *Environmental Science & Technology*, **51**, 6802–6811, 2017.

Fang, T., Hwang, B. C., Kapur, S., Hopstock, K. S., Wei, J., et al.: Wildfire particulate matter as a source of environmentally persistent free radicals and reactive oxygen species, *Environmental Science: Atmospheres*, **3**, 581–594, 2023.

Fritz, K. S. and Petersen, D. R.: An overview of the chemistry and biology of reactive aldehydes, *Free Radical Biology and Medicine*, **59**, 85–91, 2013.

Gao, D., Fang, T., Verma, V., Zeng, L., and Weber, R. J.: A method for measuring total aerosol oxidative potential (OP) with the dithiothreitol (DTT) assay and comparisons between an urban and roadside site of water-soluble and total OP, *Atmospheric Measurement Techniques*, **10**, 2821–2835, 2017.

Gligorovski, S. and Abbatt, J. P. D.: An indoor chemical cocktail, *Science*, **359**, 632–633, https://doi.org/10.1126/science.aar6837, 2018.

Go, B. R., Lyu, Y., Ji, Y., Li, Y. J., Huang, D. D., et al.: Aqueous secondary organic aerosol formation from the direct photosensitized oxidation of vanillin in the absence and presence of ammonium nitrate, *Atmospheric Chemistry and Physics*, **22**, 273–293, 2022.

Hofmann, W.: Modelling inhaled particle deposition in the human lung—A review, *Journal of Aerosol Science*, **42**, 693–724, 2011.

Hu, H., Ye, J., Liu, C., Yan, L., Yang, F., et al.: Emission and oxidative potential of PM2.5 generated by nine indoor sources, *Building and Environment*, **230**, 110021, 2023.

Indraganti, M., Boussaa, D., and Asadi, S.: Necessity of the adaptive comfort standard for the Middle East in the times of rising energy use, *Qatar Foundation Annual Research Conference Proceedings*, **EEPP3015**, 2016.

Isenor, B. H., Varnaite, G., Jeong, C.-H., Subramanian, P. G., Duruisseau-Kuntz, R., et al.: Impacts of the 2023 Canadian wildfires on the oxidative potential of particulate matter, *ACS ES&T Air*, **2**, 2238–2250, 2025.

Jareebi, M. A., Alqassim, A. Y., Almraysi, S. A., Alfaifi, W. A., Masri, T. A., et al.: Exploring the relationship between Bakhour use and respiratory health: A cross-sectional study in the Jazan Region, Saudi Arabia, *International Journal of General Medicine*, **17**, 2833–2845, 2024.

Jetter, J. J., Guo, Z., McBrian, J. A., and Flynn, M. R.: Characterization of emissions from burning incense, *Science of The Total Environment*, **295**, 51–67, https://doi.org/10.1016/S0048-9697(02)00043-8, 2002.

Jiang, H., Ahmed, C. S., Canchola, A., Chen, J. Y., and Lin, Y.-H.: Use of dithiothreitol assay to evaluate the oxidative potential of atmospheric aerosols, *Atmosphere*, **10**, 571, 2019.

Jiang, J., Jung, N., and Boor, B. E.: Using building energy and smart thermostat data to evaluate indoor ultrafine particle source and loss processes in a net-zero energy house, *ACS ES&T Engineering*, **1**, 780–793, 2021.

Kim, M., Han, C. H., and Lee, M. Y.: NADPH oxidase and the cardiovascular toxicity associated with smoking, *Toxicological Research*, **30**, 149–157, https://doi.org/10.5487/TR.2014.30.3.149, 2014.

Koch, B. P. and Dittmar, T.: From mass to structure: An aromaticity index for high-resolution mass data of natural organic matter, *Rapid Communications in Mass Spectrometry*, **20**, 926–932, 2006.

Kuye, A. and Kumar, P.: A review of the physicochemical characteristics of ultrafine particle emissions from domestic solid fuel combustion during cooking and heating, *Science of The Total Environment*, **886**, 163747, 2023.

Lai, R. W. S., Qiu, T., Zhang, X., Wang, Y., Hao, T., et al.: Deciphering the key drivers of oxidative potential during ammonium nitrate-mediated aqueous-phase photoreaction of methoxyphenols, *Atmospheric Environment*, **340**, 120895, https://doi.org/10.1016/j.atmosenv.2024.120895, 2025.

Liang, Z., Zhou, L., Chang, Y., Qin, Y., and Chan, C. K.: Biomass-burning organic aerosols as a pool of atmospheric reactive triplets to drive multiphase sulfate formation, *Proceedings of the National Academy of Sciences*, **121**, e2416803121, 2024.

Liu, F., Whitley, J., Ng, N. L., and Lu, H.: Time-resolved single-cell assay for measuring intracellular reactive oxygen species upon exposure to ambient particulate matter, *Environmental Science & Technology*, **54**, 13121–13130, https://doi.org/10.1021/acs.est.0c02889, 2020a.

Liu, F., Saavedra, M. G., Champion, J. A., Griendling, K. K., and Ng, N. L.: Prominent contribution of hydrogen peroxide to intracellular reactive oxygen species generated upon exposure to naphthalene secondary organic aerosols, *Environmental Science & Technology Letters*, **7**, 171–177, https://doi.org/10.1021/acs.estlett.9b00773, 2020b.

Liu, F., Joo, T., Ditto, J. C., Saavedra, M. G., Takeuchi, M., et al.: Oxidized and unsaturated: Key organic aerosol traits associated with cellular reactive oxygen species production in the southeastern United States, *Environmental Science & Technology*, **57**, 14150–14161, https://doi.org/10.1021/acs.est.3c03641, 2023.

Liu, X., Testa, B., and Fahr, A.: Lipophilicity and its relationship with passive drug permeation, *Pharmaceutical Research*, **28**, 962–977, 2011.

LoPachin, R. M. and Gavin, T.: Molecular mechanisms of aldehyde toxicity: A chemical perspective, *Chemical Research in Toxicology*, **27**, 1081–1091, https://doi.org/10.1021/tx5001046, 2014.

Lyu, Y., Guo, H., Cheng, T., and Li, X.: Particle size distributions of oxidative potential of lung-deposited particles: Assessing contributions from quinones and water-soluble metals, *Environmental Science & Technology*, **52**, 6592–6600, 2018.

Nazaroff, W. W. and Weschler, C. J.: Indoor ozone: Concentrations and influencing factors, *Indoor Air*, **32**, e12942, 2022.

Oberdörster, G., Oberdörster, E., and Oberdörster, J.: Nanotoxicology: An emerging discipline evolving from studies of ultrafine particles, *Environmental Health Perspectives*, **113**, 823–839, 2005.

Oh, H.-J., Chen, Y., and Kim, H.: Deposition of secondary organic aerosol in human lung model: Effect of photochemically aged aerosol on human respiratory system, *Ecotoxicology and Environmental Safety*, **265**, 115497, 2023.

Ott, W. R., Zhao, T., Cheng, K.-C., Wallace, L. A., and Hildemann, L. M.: Measuring indoor fine particle concentrations, emission rates, and decay rates from cannabis use in a residence, *Atmospheric Environment: X*, **10**, 100106, https://doi.org/10.1016/j.aeaoa.2021.100106, 2021.

Pan, A., Clark, M. L., Ang, L.-W., Yu, M. C., Yuan, J.-M., et al.: Incense use and cardiovascular mortality among Chinese in Singapore: The Singapore Chinese Health Study, *Environmental Health Perspectives*, **122**, 1279–1284, 2014.

Park, J.-H., Troxel, A. B., Harvey, R. G., and Penning, T. M.: Polycyclic aromatic hydrocarbon (PAH) o-quinones produced by the aldo-keto reductases (AKRs) generate abasic sites, oxidized pyrimidines, and 8-oxo-dGuo via reactive oxygen species, *Chemical Research in Toxicology*, **19**, 719–728, https://doi.org/10.1021/tx0600245, 2006.

Patriarca, C., Bergquist, J., Sjoberg, P. J., Tranvik, L., and Hawkes, J. A.: Online HPLC-ESI-HRMS method for the analysis and comparison of different dissolved organic matter samples, *Environmental Science & Technology*, **52**, 2091–2099, 2018.

Pillarisetti, A., Ye, W., and Chowdhury, S.: Indoor air pollution and health: Bridging perspectives from developing and developed countries, *Annual Review of Environment and Resources*, **47**, 197–229, https://doi.org/10.1146/annurev-environ-012220-010602, 2022.

Sadoun, E. T., Fthenou, E., Kakosimos, K. E., Saraga, D., and Maggos, T.: Chemical characterization of indoor and outdoor PM2.5, PM10 and VOCs in a public building in Doha City, Qatar, *Qatar Foundation Annual Research Conference Proceedings*, **EEPP1931**, 2016.

Salthammer, T.: Critical evaluation of approaches in setting indoor air quality guidelines and reference values, *Chemosphere*, **82**, 1507–1517, https://doi.org/10.1016/j.chemosphere.2010.11.023, 2011.

Seo, J., Kim, H., Park, E., Woo, J., and Lee, K.-H.: Source and condition specific toxicity of combustion-derived PM: Linking physicochemical properties with acellular and cellular assays, *Journal of Hazardous Materials*, **139344**, 2025.

Shen, G., Gaddam, C. K., Ebersviller, S. M., Vander Wal, R. L., Williams, C., et al.: A laboratory comparison of emission factors, number size distributions, and morphology of ultrafine particles from 11 different household cookstove-fuel systems, *Environmental Science & Technology*, **51**, 6522–6532, 2017.

Shultz, C. A., Quinn, A. M., Park, J.-H., Harvey, R. G., Bolton, J. L., et al.: Specificity of human aldo-keto reductases, NAD(P)H:quinone oxidoreductase, and carbonyl reductases to redox-cycle polycyclic aromatic hydrocarbon diones and 4-hydroxyequilenin-o-quinone, *Chemical Research in Toxicology*, **24**, 2153–2166, 2011.

Smith, J. S., Laskin, A., and Laskin, J.: Molecular characterization of biomass burning aerosols using high-resolution mass spectrometry, *Analytical Chemistry*, **81**, 1512–1521, 2009.

Song, J., Li, M., Zou, C., Cao, T., Fan, X., et al.: Molecular characterization of nitrogen-containing compounds in humic-like substances emitted from biomass burning and coal combustion, *Environmental Science & Technology*, **56**, 119–130, 2021.

Song, J., Li, M., Fan, X., Zou, C., Zhu, M., et al.: Molecular characterization of water- and methanol-soluble organic compounds emitted from residential coal combustion using ultrahigh-resolution electrospray ionization Fourier transform ion cyclotron resonance mass spectrometry, *Environmental Science & Technology*, **53**, 13607–13617, 2019.

Tian, Y., Arata, C., Boedicker, E., Lunderberg, D. M., Patel, S., et al.: Indoor emissions of total and fluorescent supermicron particles during HOMEChem, *Indoor Air*, **31**, 88–98, https://doi.org/10.1111/ina.12731, 2021.

Tuet, W. Y., Chen, Y., Fok, S., Gao, D., Weber, R. J., et al.: Chemical and cellular oxidant production induced by naphthalene secondary organic aerosol (SOA): Effect of redox-active metals and photochemical aging, *Scientific Reports*, **7**, 15157, 2017.

Tuet, W. Y., Fok, S., Verma, V., Rodriguez, M. S. T., Grosberg, A., et al.: Dose-dependent intracellular reactive oxygen and nitrogen species (ROS/RNS) production from particulate matter exposure: Comparison to oxidative potential and chemical composition, *Atmospheric Environment*, **144**, 335–344, 2016.

Tuet, W. Y., Liu, F., de Oliveira Alves, N., Fok, S., Artaxo, P., et al.: Chemical oxidative potential and cellular oxidative stress from open biomass burning aerosol, *Environmental Science & Technology Letters*, **6**, 126–132, https://doi.org/10.1021/acs.estlett.9b00060, 2019.

Wahab, A. A. and Mostafa, O. A.: Arabian incense exposure among Qatari asthmatic children: A possible risk factor, *Saudi Medical Journal*, **28**, 476–478, 2007.

Wang, C., Collins, D. B., Hems, R. F., Borduas, N., Antiñolo, M., et al.: Exploring conditions for ultrafine particle formation from oxidation of cigarette smoke in indoor environments, *Environmental Science & Technology*, **52**, 4623–4631, 2018a.

Wang, K., Huang, R.-J., Brüggemann, M., Zhang, Y., Yang, L., et al.: Urban organic aerosol composition in eastern China differs from north to south: Molecular insight from a liquid chromatography–mass spectrometry (Orbitrap) study, *Atmospheric Chemistry and Physics*, **21**, 9089–9104, 2021.

Wang, S., Ye, J., Soong, R., Wu, B., Yu, L., et al.: Relationship between chemical composition and oxidative potential of secondary organic aerosol from polycyclic aromatic hydrocarbons, *Atmospheric Chemistry and Physics*, **18**, 3987–4003, 2018b.

Wang, S., Gallimore, P. J., Liu-Kang, C., Yeung, K., Campbell, S. J., et al.: Dynamic wood smoke aerosol toxicity during oxidative atmospheric aging, *Environmental Science & Technology*, **57**, 1246–1256, 2023.

Wang, X. and Chan, A. W.: Particulate matter and volatile organic compound emissions generated from a domestic air fryer, *Environmental Science & Technology*, **57**, 17384–17392, 2023.

Wong, J. P., Tsagkaraki, M., Tsiodra, I., Mihalopoulos, N., Violaki, K., et al.: Effects of atmospheric processing on the oxidative potential of biomass burning organic aerosols, *Environmental Science & Technology*, **53**, 6747–6756, 2019.

Wu, C. L., Chao, C. Y. H., Sze-To, G. N., Wan, M. P., and Chan, T. C.: Ultrafine particle emissions from cigarette smouldering, incense burning, vacuum cleaner motor operation and cooking, *Indoor and Built Environment*, **21**, 782–796, https://doi.org/10.1177/1420326X11421356, 2012.

Xiong, Q., Yu, H., Wang, R., Wei, J., and Verma, V.: Rethinking dithiothreitol-based particulate matter oxidative potential: Measuring dithiothreitol consumption versus reactive oxygen species generation, *Environmental Science & Technology*, **51**, 6507–6514, 2017.

Yeatts, K. B., El-Sadig, M., Leith, D., Kalsbeek, W., Al-Maskari, F., et al.: Indoor air pollutants and health in the United Arab Emirates, *Environmental Health Perspectives*, **120**, 687–694, 2012.

Yuan, W., Zhang, L., Zhao, W., Yang, B., Jiao, X., et al.: Multiphase reaction of ozone with HONO/NO2− on surfaces: Effects on indoor HONO and ozone, *Environmental Science & Technology*, **59**, 7246–7255, 2025.

Zhang, L., Li, Y., Li, J., Xing, R., Liu, X., et al.: Pollutant emissions and oxidative potentials of particles from the indoor burning of biomass pellets, *Environmental Science & Technology*, **58**, 16016–16027, 2024.

Zhang, Y., McMurry, P. H., Yu, F., and Jacobson, M. Z.: A comparative study of nucleation parameterizations: 1. Examination and evaluation of the formulations, *Journal of Geophysical Research: Atmospheres*, **115**, 2010.

Zhao, L. and Liu, J.: Operating behavior and corresponding performance of mechanical ventilation systems in Chinese residential buildings, *Building and Environment*, **170**, 106600, https://doi.org/10.1016/j.buildenv.2019.106600, 2020.

Zhao, W., Jiao, X., Xie, Y., Liu, T., Zhou, L., et al.: Impact of mosquito-repellent incense emissions and aging processes in the indoor environment, *ACS ES&T Air*, **2**, 2659–2668, 2025.

Abbatt, J. P. and Wang, C.: The atmospheric chemistry of indoor environments, Environmental Science: Processes & Impacts, 22, 25-48, 2020.

Al-Rawas, O. A., Al-Maniri, A. A., and Al-Riyami, B. M.: Home exposure to Arabian incense (bakhour) and asthma symptoms in children: a community survey in two regions in Oman, BMC pulmonary medicine, 9, 23, 2009.

Alarifi, S. A., Mubarak, M. M., and Alokail, M. S.: Ultrastructural changes of pneumocytes of rat exposed to Arabian incense (Bakhour), Saudi Med J, 25, 1689-1693, 2004.

Ault, A. P., Grassian, V. H., Carslaw, N., Collins, D. B., Destaillats, H., et al.: Indoor surface chemistry: developing a molecular picture of reactions on indoor interfaces, Chem, 6, 3203-3218, 2020.

Brehmer, C., Lai, A., Clark, S., Shan, M., Ni, K., et al.: The oxidative potential of personal and household PM2. 5 in a rural setting in southwestern China, Environmental science & technology, 53, 2788-2798, 2019.

Browne, C., Keith, C., and Allen, R.: The effect of filter ventilation on the yield and composition of mainstream and sidestream smokes, Beitr. Tabakforsch. Int, 10, 81-90, 1980.

Bu-Olayan, A. H. and Thomas, B. V.: Exposition of respiratory ailments from trace metals concentrations in incenses, Scientific Reports, 11, 10210, 10.1038/s41598-021-89493-w, 2021.

Charrier, J. G. and Anastasio, C.: On dithiothreitol (DTT) as a measure of oxidative potential for ambient particles: evidence for the importance of soluble transition metals, Atmospheric chemistry and physics (Print), 12, 11317, 2012.

Charrier, J. G., McFall, A. S., Vu, K. K., Baroi, J., Olea, C., et al.: A bias in the "mass-normalized" DTT response–An effect of non-linear concentration-response curves for copper and manganese, Atmospheric Environment, 144, 325-334, 2016.

Chen, C. and Zhao, B.: Indoor Emissions Contributed the Majority of Ultrafine Particles in Chinese Urban Residences, Environmental Science & Technology, 58, 8444-8456, 10.1021/acs.est.4c00556, 2024.

Chen, K., Raeofy, N., Lum, M., Mayorga, R., Woods, M., et al.: Solvent effects on chemical composition and optical properties of extracted secondary brown carbon constituents, Aerosol Science and Technology, 56, 917-930, 2022.

Cho, A. K., Sioutas, C., Miguel, A. H., Kumagai, Y., Schmitz, D. A., et al.: Redox activity of airborne particulate matter at different sites in the Los Angeles Basin, Environmental research, 99, 40-47, 2005.

Chuang, H.-C., BéruBé, K., Lung, S.-C. C., Bai, K.-J., and Jones, T.: Investigation into the oxidative potential generated by the formation of particulate matter from incense combustion, Journal of Hazardous Materials, 244-245, 142-150, https://doi.org/10.1016/j.jhazmat.2012.11.034, 2013.

Cincinelli, A. and Martellini, T.: Indoor air quality and health, 2017.

Cohen, R., Sexton, K. G., and Yeatts, K. B.: Hazard assessment of United Arab Emirates (UAE) incense smoke, Science of the total environment, 458, 176-186, 2013.

Dalibalta, S., Elsayed, Y., Alqtaishat, F., Gomes, I., and Fernandes, N.: A health risk assessment of Arabian incense (Bakhour) smoke in the United Arab Emirates, Science of The Total Environment, 511, 684-691, https://doi.org/10.1016/j.scitotenv.2014.12.024, 2015.

DeCarlo, P. F., Slowik, J. G., Worsnop, D. R., Davidovits, P., and Jimenez, J. L.: Particle morphology and density characterization by combined mobility and aerodynamic diameter measurements. Part 1: Theory, Aerosol Science and Technology, 38, 1185-1205, 2004.
Dewald, P., Lelieveld, J., and Crowley, J. N.: NO 3 reactivity measurements in an indoor environment: a pilot study, Environmental Science: Atmospheres, 3, 1778-1790, 2023.
Diapouli, E., Chaloulakou, A., and Koutrakis, P.: Estimating the concentration of indoor particles of outdoor origin: A review, Journal of the Air & Waste Management Association, 63, 1113-1129, 2013.
Dou, J., Lin, P., Kuang, B.-Y., and Yu, J. Z.: Reactive Oxygen Species Production Mediated by Humic-like Substances in Atmospheric Aerosols: Enhancement Effects by Pyridine, Imidazole, and Their Derivatives, Environmental Science & Technology, 49, 6457-6465, 10.1021/es5059378, 2015.
Elsayed, Y., Dalibalta, S., Gomes, I., Fernandes, N., and Alqtaishat, F.: Chemical composition and potential health risks of raw Arabian incense (Bakhour), Journal of Saudi Chemical Society, 20, 465-473, 2016.
Escalante, J., Chen, W.-H., Tabatabaei, M., Hoang, A. T., Kwon, E. E., et al.: Pyrolysis of lignocellulosic, algal, plastic, and other biomass wastes for biofuel production and circular bioeconomy: A review of thermogravimetric analysis (TGA) approach, Renewable and Sustainable Energy Reviews, 169, 112914, 2022.
Fang, T., Zeng, L., Gao, D., Verma, V., Stefaniak, A. B., et al.: Ambient size distributions and lung deposition of aerosol dithiothreitol-measured oxidative potential: contrast between soluble and insoluble particles, Environmental Science & Technology, 51, 6802-6811, 2017.
Fang, T., Hwang, B. C., Kapur, S., Hopstock, K. S., Wei, J., et al.: Wildfire particulate matter as a source of environmentally persistent free radicals and reactive oxygen species, Environmental Science: Atmospheres, 3, 581-594, 2023.
Fritz, K. S. and Petersen, D. R.: An overview of the chemistry and biology of reactive aldehydes, Free Radical Biology and Medicine, 59, 85-91, 2013.
Gao, D., Fang, T., Verma, V., Zeng, L., and Weber, R. J.: A method for measuring total aerosol oxidative potential (OP) with the dithiothreitol (DTT) assay and comparisons between an urban and roadside site of water-soluble and total OP, Atmospheric Measurement Techniques, 10, 2821-2835, 2017.
Gligorovski, S. and Abbatt, J. P. D.: An indoor chemical cocktail, Science, 359, 632-633, doi:10.1126/science.aar6837, 2018.
Go, B. R., Lyu, Y., Ji, Y., Li, Y. J., Huang, D. D., et al.: Aqueous secondary organic aerosol formation from the direct photosensitized oxidation of vanillin in the absence and presence of ammonium nitrate, Atmospheric Chemistry and Physics, 22, 273-293, 2022.
Hinds, W. C. and Zhu, Y.: Aerosol technology: properties, behavior, and measurement of airborne particles, John Wiley & Sons2022.
Hofmann, W.: Modelling inhaled particle deposition in the human lung—A review, Journal of Aerosol Science, 42, 693-724, 2011.
Hu, H., Ye, J., Liu, C., Yan, L., Yang, F., et al.: Emission and oxidative potential of PM2. 5 generated by nine indoor sources, Building and Environment, 230, 110021, 2023.
Indraganti, M., Boussaa, D., and Asadi, S.: Necessity of the Adaptive Comfort Standard for the Middle East in the Times of Rising Energy Use, 2016, https://doi.org/10.5339/qfarc.2016.EEPP3015, 2016.
Jareebi, M. A., Alqassim, A. Y., Almraysi, S. A., Alfaifi, W. A., Masri, T. A., et al.: Exploring the Relationship Between Bakhour Use and Respiratory Health: A Cross-Sectional Study in the Jazan Region, Saudi Arabia, International Journal of General Medicine, 2833-2845, 2024.
Jetter, J. J., Guo, Z., McBrian, J. A., and Flynn, M. R.: Characterization of emissions from burning incense, Science of The Total Environment, 295, 51-67, https://doi.org/10.1016/S0048-9697(02)00043-8, 2002.
Ji, X., Le Bihan, O., Ramalho, O., Mandin, C., D'Anna, B., et al.: Characterization of particles emitted by incense burning in an experimental house, Indoor Air, 20, 147-158, 2010.
Jiang, H., Ahmed, C. S., Canchola, A., Chen, J. Y., and Lin, Y.-H.: Use of dithiothreitol assay to evaluate the oxidative potential of atmospheric aerosols, Atmosphere, 10, 571, 2019.
Jiang, J., Jung, N., and Boor, B. E.: Using building energy and smart thermostat data to evaluate indoor ultrafine particle source and loss processes in a net-zero energy house, ACS ES&T Engineering, 1, 780-793, 2021.
Kim, M., Han, C. H., and Lee, M. Y.: NADPH oxidase and the cardiovascular toxicity associated with smoking, Toxicol Res, 30, 149-157, 10.5487/tr.2014.30.3.149, 2014.

Klosterköther, A., Kurtenbach, R., Wiesen, P., and Kleffmann, J.: Determination of the emission indices for NO, NO2, HONO, HCHO, CO, and particles emitted from candles, Indoor Air, 31, 116-127, 2021.
Koch, B. P. and Dittmar, T.: From mass to structure: An aromaticity index for high-resolution mass data of natural organic matter, Rapid communications in mass spectrometry, 20, 926-932, 2006.
Ku, B. K. and Maynard, A. D.: Comparing aerosol surface-area measurements of monodisperse ultrafine silver agglomerates by mobility analysis, transmission electron microscopy and diffusion charging, Journal of aerosol science, 36, 1108-1124, 2005.
Kuye, A. and Kumar, P.: A review of the physicochemical characteristics of ultrafine particle emissions from domestic solid fuel combustion during cooking and heating, Science of The Total Environment, 886, 163747, 2023.
Lai, R. W. S., Qiu, T., Zhang, X., Wang, Y., Hao, T., et al.: Deciphering the key drivers of oxidative potential during ammonium nitrate-mediated aqueous-phase photoreaction of methoxyphenols, Atmospheric Environment, 340, 120895, https://doi.org/10.1016/j.atmosenv.2024.120895, 2025.
Lee, A. K., Chan, C. K., Fang, M., and Lau, A. P.: The 3-hydroxy fatty acids as biomarkers for quantification and characterization of endotoxins and Gram-negative bacteria in atmospheric aerosols in Hong Kong, Atmospheric Environment, 38, 6307-6317, 2004.
Levin, M., Witschger, O., Bau, S., Jankowska, E., Koponen, I. K., et al.: Can we trust real time measurements of lung deposited surface area concentrations in dust from powder nanomaterials?, Aerosol and Air Quality Research, 16, 1105-1117, 2016.
Liang, Z., Zhou, L., Chang, Y., Qin, Y., and Chan, C. K.: Biomass-burning organic aerosols as a pool of atmospheric reactive triplets to drive multiphase sulfate formation, Proceedings of the National Academy of Sciences, 121, e2416803121, 2024.
Liigand, P., Kaupmees, K., Haav, K., Liigand, J., Leito, I., et al.: Think negative: finding the best electrospray ionization/MS mode for your analyte, Analytical chemistry, 89, 5665-5668, 2017.
Lionetto, M. G., Guascito, M. R., Giordano, M. E., Caricato, R., De Bartolomeo, A. R., et al.: Oxidative potential, cytotoxicity, and intracellular oxidative stress generating capacity of PM10: A case study in South of Italy, Atmosphere, 12, 464, 2021.
Liu, F., Whitley, J., Ng, N. L., and Lu, H.: Time-Resolved Single-Cell Assay for Measuring Intracellular Reactive Oxygen Species upon Exposure to Ambient Particulate Matter, Environmental Science & Technology, 54, 13121-13130, 10.1021/acs.est.0c02889, 2020a.
Liu, F., Saavedra, M. G., Champion, J. A., Griendling, K. K., and Ng, N. L.: Prominent Contribution of Hydrogen Peroxide to Intracellular Reactive Oxygen Species Generated upon Exposure to Naphthalene Secondary Organic Aerosols, Environmental Science & Technology Letters, 7, 171-177, 10.1021/acs.estlett.9b00773, 2020b.
Liu, F., Joo, T., Ditto, J. C., Saavedra, M. G., Takeuchi, M., et al.: Oxidized and Unsaturated: Key Organic Aerosol Traits Associated with Cellular Reactive Oxygen Species Production in the Southeastern United States, Environmental Science & Technology, 57, 14150-14161, 10.1021/acs.est.3c03641, 2023.
Liu, X., Testa, B., and Fahr, A.: Lipophilicity and its relationship with passive drug permeation, Pharmaceutical research, 28, 962-977, 2011.
LoPachin, R. M. and Gavin, T.: Molecular mechanisms of aldehyde toxicity: a chemical perspective, Chem Res Toxicol, 27, 1081-1091, 10.1021/tx5001046, 2014.
Lyu, Y., Guo, H., Cheng, T., and Li, X.: Particle size distributions of oxidative potential of lung-deposited particles: assessing contributions from quinones and water-soluble metals, Environmental Science & Technology, 52, 6592-6600, 2018.
Maitra, U., Singh, N., Gan, L., Ringwood, L., and Li, L.: IRAK-1 contributes to lipopolysaccharide-induced reactive oxygen species generation in macrophages by inducing NOX-1 transcription and Rac1 activation and suppressing the expression of antioxidative enzymes, Journal of Biological Chemistry, 284, 35403-35411, 2009.
Nazaroff, W. W. and Weschler, C. J.: Indoor ozone: Concentrations and influencing factors, Indoor air, 32, e12942, 2022.
Oberdörster, G., Oberdörster, E., and Oberdörster, J.: Nanotoxicology: an emerging discipline evolving from studies of ultrafine particles, Environmental health perspectives, 113, 823, 2005.
Oh, H.-J., Chen, Y., and Kim, H.: Deposition of secondary organic aerosol in human lung model: effect of photochemically aged aerosol on human respiratory system, Ecotoxicology and Environmental Safety, 265, 115497, 2023.

Ott, W. R., Zhao, T., Cheng, K.-C., Wallace, L. A., and Hildemann, L. M.: Measuring indoor fine particle concentrations, emission rates, and decay rates from cannabis use in a residence, Atmospheric Environment: X, 10, 100106, https://doi.org/10.1016/j.aeaoa.2021.100106, 2021.
Pan, A., Clark, M. L., Ang, L.-W., Yu, M. C., Yuan, J.-M., et al.: Incense use and cardiovascular mortality among Chinese in Singapore: the Singapore Chinese Health Study, Environmental health perspectives, 122, 1279, 2014.
Park, J.-H., Troxel, A. B., Harvey, R. G., and Penning, T. M.: Polycyclic Aromatic Hydrocarbon (PAH) o-Quinones Produced by the Aldo-Keto-Reductases (AKRs) Generate Abasic Sites, Oxidized Pyrimidines, and 8-Oxo-dGuo via Reactive Oxygen Species, Chemical Research in Toxicology, 19, 719-728, 10.1021/tx0600245, 2006.
Patriarca, C., Bergquist, J., Sjoberg, P. J., Tranvik, L., and Hawkes, J. A.: Online HPLC-ESI-HRMS method for the analysis and comparison of different dissolved organic matter samples, Environmental science & technology, 52, 2091-2099, 2018.
Pillarisetti, A., Ye, W., and Chowdhury, S.: Indoor Air Pollution and Health: Bridging Perspectives from Developing and Developed Countries, Annual Review of Environment and Resources, 47, 197-229, https://doi.org/10.1146/annurev-environ-012220-010602, 2022.
Sadoun, E. T., Fthenou, E., Kakosimos, K., Saraga, D., and Maggos, T.: Chemical Characterization of Indoor and Outdoor PM2.5, PM10 and VOCs in a Public Building in Doha City, Qatar, 2016, https://doi.org/10.5339/qfarc.2016.EEPP1931, 2016.
Salthammer, T.: Critical evaluation of approaches in setting indoor air quality guidelines and reference values, Chemosphere, 82, 1507-1517, 2011.
Sanlioglu, S., Williams, C. M., Samavati, L., Butler, N. S., Wang, G., et al.: Lipopolysaccharide induces Rac1-dependent reactive oxygen species formation and coordinates tumor necrosis factor-α secretion through IKK regulation of NF-κB, Journal of Biological Chemistry, 276, 30188-30198, 2001.
Seinfeld, J. H. and Pandis, S. N.: Atmospheric chemistry and physics: from air pollution to climate change, John Wiley & Sons2016.
Seo, J., Kim, H., Park, E., Woo, J., and Lee, K.-H.: Source and condition specific toxicity of combustion-derived PM: Linking physicochemical properties with acellular and cellular assays, Journal of hazardous materials, 139344, 2025.
Shen, G., Gaddam, C. K., Ebersviller, S. M., Vander Wal, R. L., Williams, C., et al.: A laboratory comparison of emission factors, number size distributions, and morphology of ultrafine particles from 11 different household cookstove-fuel systems, Environmental science & technology, 51, 6522-6532, 2017.
Shultz, C. A., Quinn, A. M., Park, J.-H., Harvey, R. G., Bolton, J. L., et al.: Specificity of human aldo-keto reductases, NAD(P)H:quinone oxidoreductase, and carbonyl reductases to redox-cycle polycyclic aromatic hydrocarbon diones and 4-hydroxyequilenin-o-quinone, Chemical research in toxicology, 24 12, 2153-2166, 2011.
Smith, J. S., Laskin, A., and Laskin, J.: Molecular characterization of biomass burning aerosols using high-resolution mass spectrometry, Analytical chemistry, 81, 1512-1521, 2009.
Song, J., Li, M., Zou, C., Cao, T., Fan, X., et al.: Molecular characterization of nitrogen-containing compounds in humic-like substances emitted from biomass burning and coal combustion, Environmental Science & Technology, 56, 119-130, 2021.
Song, J., Li, M., Fan, X., Zou, C., Zhu, M., et al.: Molecular characterization of water-and methanol-soluble organic compounds emitted from residential coal combustion using ultrahigh-resolution electrospray ionization Fourier transform ion cyclotron resonance mass spectrometry, Environmental Science & Technology, 53, 13607-13617, 2019.
Tian, Y., Arata, C., Boedicker, E., Lunderberg, D. M., Patel, S., et al.: Indoor emissions of total and fluorescent supermicron particles during HOMEChem, Indoor Air, 31, 88-98, https://doi.org/10.1111/ina.12731, 2021.
Tsuji, K. and Harrison, S. J.: Dry-heat destruction of lipopolysaccharide: dry-heat destruction kinetics, Applied and environmental microbiology, 36, 710-714, 1978.
Tuet, W. Y., Chen, Y., Fok, S., Gao, D., Weber, R. J., et al.: Chemical and cellular oxidant production induced by naphthalene secondary organic aerosol (SOA): effect of redox-active metals and photochemical aging, Scientific reports, 7, 15157, 2017.

Tuet, W. Y., Fok, S., Verma, V., Rodriguez, M. S. T., Grosberg, A., et al.: Dose-dependent intracellular reactive oxygen and nitrogen species (ROS/RNS) production from particulate matter exposure: comparison to oxidative potential and chemical composition, Atmospheric Environment, 144, 335-344, 2016.
Tuet, W. Y., Liu, F., de Oliveira Alves, N., Fok, S., Artaxo, P., et al.: Chemical Oxidative Potential and Cellular Oxidative Stress from Open Biomass Burning Aerosol, Environmental Science & Technology Letters, 6, 126-132, 10.1021/acs.estlett.9b00060, 2019.
Wahab, A. A. and Mostafa, O. A.: Arabian incense exposure among Qatari asthmatic children. A possible risk factor, 2007.
Wallace, L.: Indoor sources of ultrafine and accumulation mode particles: size distributions, size-resolved concentrations, and source strengths, Aerosol science and technology, 40, 348-360, 2006.
Wang, C., Collins, D. B., Hems, R. F., Borduas, N., Antiñolo, M., et al.: Exploring conditions for ultrafine particle formation from oxidation of cigarette smoke in indoor environments, Environmental Science & Technology, 52, 4623-4631, 2018a.
Wang, K., Huang, R.-J., Brüggemann, M., Zhang, Y., Yang, L., et al.: Urban organic aerosol composition in eastern China differs from north to south: molecular insight from a liquid chromatography–mass spectrometry (Orbitrap) study, Atmospheric Chemistry and Physics, 21, 9089-9104, 2021.
Wang, S., Ye, J., Soong, R., Wu, B., Yu, L., et al.: Relationship between chemical composition and oxidative potential of secondary organic aerosol from polycyclic aromatic hydrocarbons, Atmospheric Chemistry and Physics, 18, 3987-4003, 2018b.
Wang, S., Gallimore, P. J., Liu-Kang, C., Yeung, K., Campbell, S. J., et al.: Dynamic wood smoke aerosol toxicity during oxidative atmospheric aging, Environmental Science & Technology, 57, 1246-1256, 2023.
Wang, X. and Chan, A. W.: Particulate matter and volatile organic compound emissions generated from a domestic air fryer, Environmental Science & Technology, 57, 17384-17392, 2023.
Waring, M. S. and Wells, J. R.: Volatile organic compound conversion by ozone, hydroxyl radicals, and nitrate radicals in residential indoor air: Magnitudes and impacts of oxidant sources, Atmospheric Environment, 106, 382-391, 2015.
Weschler, C. J. and Carslaw, N.: Indoor chemistry, Environmental Science & Technology, 52, 2419-2428, 2018.
Wong, J. P., Tsagkaraki, M., Tsiodra, I., Mihalopoulos, N., Violaki, K., et al.: Effects of atmospheric processing on the oxidative potential of biomass burning organic aerosols, Environmental science & technology, 53, 6747-6756, 2019.
Wu, C. L., Chao, C. Y. H., Sze-To, G. N., Wan, M. P., and Chan, T. C.: Ultrafine Particle Emissions from Cigarette Smouldering, Incense Burning, Vacuum Cleaner Motor Operation and Cooking, Indoor and Built Environment, 21, 782-796, 10.1177/1420326x11421356, 2012.
Xiong, Q., Yu, H., Wang, R., Wei, J., and Verma, V.: Rethinking dithiothreitol-based particulate matter oxidative potential: measuring dithiothreitol consumption versus reactive oxygen species generation, Environmental science & technology, 51, 6507-6514, 2017.
Yeatts, K. B., El-Sadig, M., Leith, D., Kalsbeek, W., Al-Maskari, F., et al.: Indoor air pollutants and health in the United Arab Emirates, Environmental health perspectives, 120, 687, 2012.
Yuan, W., Zhang, L., Zhao, W., Yang, B., Jiao, X., et al.: Multiphase Reaction of Ozone with HONO/NO2–on Surfaces: Effects on Indoor HONO and Ozone, Environmental Science & Technology, 59, 7246-7255, 2025.
Zannoni, N., Lakey, P. S., Won, Y., Shiraiwa, M., Rim, D., et al.: The human oxidation field, Science, 377, 1071-1077, 2022.
Zhang, Y., McMurry, P. H., Yu, F., and Jacobson, M. Z.: A comparative study of nucleation parameterizations: 1. Examination and evaluation of the formulations, Journal of Geophysical Research: Atmospheres, 115, 2010.
Zhao, L. and Liu, J.: Operating behavior and corresponding performance of mechanical ventilation systems in Chinese residential buildings, Building and Environment, 170, 106600, https://doi.org/10.1016/j.buildenv.2019.106600, 2020.
Zhao, W., Jiao, X., Xie, Y., Liu, T., Zhou, L., et al.: Impact of Mosquito-Repellent Incense Emissions and Aging Processes in the Indoor Environment, ACS ES&T Air, 2, 2659-2668, 2025.